

Chapter 10. Towards a Thermodynamics of Steady States



- 10.1 Introduction
- 10.2 Chaotic Dynamical Systems
- 10.3 The Characterization of Chaos
- 10.4 Chaos in planar Couette flow
- 10.5 Green's expansion for the entropy

10.1 Introduction

In the previous three chapters we have developed a theory which can be applied to calculate the nonlinear response of an arbitrary phase variable to an applied external field. We have described several different representations for the N-particle, nonequilibrium distribution function, $f(\mathbf{\Gamma},t)$: the Kubo representation (§7.1) which is only useful from a formal point of view; and two related representations, the Transient Time Correlation Function formalism (§7.3) and the Kawasaki representation (§7.2), both of which can be applied to obtain useful results. We now turn our interest towards thermodynamic properties which are not simple phase averages but rather are functionals of the distribution function itself. We will consider the entropy and free energy of nonequilibrium steady states. At this point it is useful to recall the connections between equilibrium statistical mechanics, the thermodynamic entropy (Gibbs, 1902), and Boltzmann's famous H theorem (1872). Gibbs pointed out that *at equilibrium*, the entropy of a classical N-particle system can be calculated from the relation,

$$S(t) = -k_B \int d\mathbf{\Gamma} f(\mathbf{\Gamma}) \log f(\mathbf{\Gamma}) \quad (10.1.1)$$

where $f(\mathbf{\Gamma})$ is a time independent equilibrium distribution function. Using the same equation, Boltzmann calculated the *nonequilibrium* entropy of gases in the low density limit . He showed that if one uses the single particle distribution of velocities obtained from the irreversible Boltzmann equation, the entropy of a gas at equilibrium is greater than that of any nonequilibrium gas with the same number of particles, volume and energy. Furthermore he showed that the Boltzmann equation predicts a *monotonic* increase in the entropy of an isolated gas as it relaxes towards equilibrium. These results are the content of his famous H-theorem (Huang, 1963). They are in accord with our intuition that the increase in entropy is the driving force behind the relaxation to equilibrium.

One can use the reversible Liouville equation to calculate the change in the entropy of a dense many body system. Suppose we consider a Gaussian isokinetic system subject to a time independent external field F_e , (8.10.2). We expect that the entropy of a nonequilibrium steady state will be finite and less than that of the corresponding equilibrium system with the same energy. From (10.1.1) we see that,

$$\dot{S} = -k_B \int d\mathbf{\Gamma} [1 + \ln f] \frac{\partial f}{\partial t} \quad (10.1.2)$$

Using successive integrations by parts one finds for an N-particle system in 3 dimensions,

$$\begin{aligned}
\dot{S} &= -k_B \int d\Gamma f \dot{\Gamma} \cdot \frac{\partial}{\partial \Gamma} [1 + \ln f] \\
&= -k_B \int d\Gamma \dot{\Gamma} \cdot \frac{\partial f}{\partial \Gamma} \\
&= k_B \int d\Gamma f(t) \frac{\partial}{\partial \Gamma} \cdot \dot{\Gamma} = -3Nk_B \langle \alpha(t) \rangle
\end{aligned} \tag{10.1.3}$$

Now for any nonequilibrium steady state, the average of the Gaussian multiplier α , is positive. The external field does work on the system which must be removed by the thermostat. This means that the Liouville equation predicts that the Gibbs entropy (10.1.1), diverges to negative infinity! After the decay of initial transients (10.1.3) shows the rate of decrease of the entropy is constant. This paradoxical result was first derived by Evans (1985). If there is no thermostat, the Liouville equation predicts that the Gibbs entropy of an arbitrary system, satisfying $A\dot{\Gamma}$ and subject to an external dissipative field, is constant! This result was known to Gibbs (1902).

Gibbs went on to show that if one computes a coarse grained entropy, by limiting the resolution with which we compute the distribution function, then the coarse grained entropy based on (10.1.1), obeys a generalized H-theorem. He showed that the coarse grained entropy cannot decrease (Gibbs, 1902). We shall return to the question of coarse graining in §10.5.

The reason for the divergence in (10.1.3) is not difficult to find. Consider a small region of phase space, $d\Gamma$, at $t=0$, when the field is turned on. If we follow the phase trajectory of a point originally within $d\Gamma$, the local relative density of ensemble points in phase space about $\Gamma(t)$ can be calculated from the Liouville equation,

$$\frac{1}{f(t)} \frac{df(t)}{dt} = 3N\alpha(t) \tag{10.1.4}$$

If the external field is sufficiently large we know that there will be some trajectories along which the multiplier, $\alpha(t)$, is positive for **all** time. For such trajectories equation (10.1.4) predicts that the local density of the phase space distribution function must diverge in time, towards positive infinity. The distribution function of a steady state will be singular at long times. One way in which this could happen would be for the distribution function to evolve into a space of lower dimension than the *ostensible* $6N$ dimensions of phase space. If the dimension of the phase space which is *accessible* to nonequilibrium steady states is lower than the ostensible dimension, the volume of accessible phase space (as computed from within the ostensible phase space), will be zero. If this were so, the Gibbs entropy of the system (which occupies zero volume in ostensible phase space) would be minus infinity.

At this stage these arguments are not at all rigorous. We have yet to define what we mean by a continuous change in the dimension. In the following sections we will show that a

reduction in the dimension of accessible phase space is a universal feature of nonequilibrium steady states. The phase space trajectories are chaotic and separate exponentially with time, and for nonequilibrium systems, the accessible steady state phase space is a strange attractor whose dimension is less than that of the initial equilibrium phase space. These ideas are new and the relations between them and nonlinear response theory are yet to develop. We feel however, that the ideas and insights already gleaned are sufficiently important to present here.

Before we start a detailed analysis it is instructive to consider two classic problems from the new science of dynamical systems - the quadratic map and the Lorenz model. This will introduce many of the concepts needed later to quantitatively characterize nonequilibrium steady states.

10.2 Chaotic Dynamical Systems

The study of low dimensional dynamical systems which exhibit chaos is a very active area of current research. A very useful introductory account can be found in Schuster (1988). It was long thought that the complex behavior of systems of many degrees of freedom was inherently different to that of simple mechanical systems. It is now known that simple one dimensional nonlinear systems can indeed show very complex behavior. For example the family of quadratic maps $F_{\mu}(x)=\mu x(1-x)$ demonstrates many of these features. This is very well described in a recent book by Devaney (1986). The connection between a discrete mapping, and the solution of a system of ordinary differential equations in a molecular dynamics simulation is clear when we realise that the numerical solution of the equations of motion for a system involves an iterative mapping of points in phase space. Although we are solving a problem which is continuous in time, the differential equation solver transforms this into a discrete time problem. The result is that if the mapping f takes $\Gamma(0)$ to $\Gamma(\Delta)$ where Δ is the time step, then $\Gamma(n\Delta) = f^n[\Gamma(0)]$. Here f^n means the composite mapping consisting of n repeated operations of f , $f[f[\dots f[\Gamma(0)]]\dots]$.

An important difference exists between difference equations and similar differential equations, for example if consider the differential equation

$$\frac{dx}{dt} = \mu x (1 - x) \quad (10.2.1)$$

the solution can easily be obtained

$$x(t) = \frac{x_0 e^{\mu t}}{1 - x_0 + x_0 e^{\mu t}} \quad (10.2.2)$$

where $x_0=x(t=0)$. The trajectory for this system is now quite straightforward to understand. The solution of the quadratic map difference equation is a much more difficult problem which is still not completely understood.

The Quadratic Map

The quadratic map is defined by the equation

$$x_{n+1} = F_{\mu}(x_n) = \mu x_n (1 - x_n) \quad (10.2.3)$$

If we iterate this mapping for $\mu=4$, starting with a random number in the interval between 0 and 1, then we obtain dramatically different behavior depending upon the initial value of x . Sometimes the values repeat; other times they do not; and usually they wander about in the range 0 to 1. Initial values of x which are quite close together can have dramatically different iterates. This

unpredictability or sensitive dependence on initial conditions is a property familiar in statistical mechanical simulations of higher dimensional systems. If we change the map to $x_{n+1}=3.839x_n(1-x_n)$ then a random initial value of x leads to a repeating cycle of three numbers (0.149888...,0.489172...,0.959299...). This mapping includes a set of initial values which behave just as unpredictably as those in the $\mu=4$ example but due to round-off error we don't see this randomness.

Before we look at the more complicated behavior we consider some of the simpler properties of the family of quadratic maps. First we require some definitions; x_1 is called a fixed point of the map f if $f(x_1) = x_1$. x_1 is a periodic point, of period n , if $f^n(x_1) = x_1$, where f^n represents n applications of the mapping f . Clearly a fixed point is a periodic point of period one. The fixed point at x_1 is stable if $|f'(x_1)| < 1$. We will consider the quadratic map $F_\mu(x)$ on the interval $0 < x < 1$, as a function of the parameter μ .

Region 1 $0 < \mu < 1$

The mapping $F_\mu(x)$ has only one fixed point $x=0$. $F'_\mu(0) = \mu$ so in this region the fixed point at $x=0$ is attracting (or stable).

Region 2 $1 < \mu < 3$

$F_\mu(x)$ has two fixed points $x=0$ and $x_p=(\mu-1)/\mu$. The fixed point $x=0$ is repelling (or unstable) while $F'_\mu(x_p) = 2-\mu$ so that x_p is an attracting (or stable) fixed point.

Region 3 $3 < \mu < 1+\sqrt{6}$

In this region both the fixed points of $F_\mu(x)$ are unstable so it is useful to consider the composite mapping $F_\mu^2(x) = F_\mu(F_\mu(x)) = \mu^2x(1-x)[1-\mu x(1-x)]$. F_μ^2 has the fixed points of the original mapping $F_\mu(x)$ at $x=0$ and x_p , but as before both of these are unstable. F_μ^2 also has two new fixed points at $x_\pm = \{1 \pm [(\mu-3)/(\mu+1)]^{1/2}\}(\mu+1)/2\mu$. These two fixed points x_\pm of F_μ^2 are points of period two in the original mapping $F_\mu(x)$, (referred to as a 2-cycle). $(F_\mu^2)'(x_\pm) = 4+2\mu-\mu^2$ so the 2-cycle is stable for $3 < \mu < 1+\sqrt{6}$.

Region 4,5, etc $1+\sqrt{6} < \mu < \mu_\infty$

The period doubling cascade where the stable 2-cycle loses its stability, and a stable 4-cycle appears; increasing μ the 4-cycle loses stability and is replaced by a stable 8-cycle; increasing μ again leads to the breakdown of the 2^{n-1} -cycle and the emergence of a stable 2^n -cycle. The μ bifurcation values get closer and closer together, and the limit as $n \rightarrow \infty$ the bifurcation value is approximately $\mu_\infty = 3.5699456$.

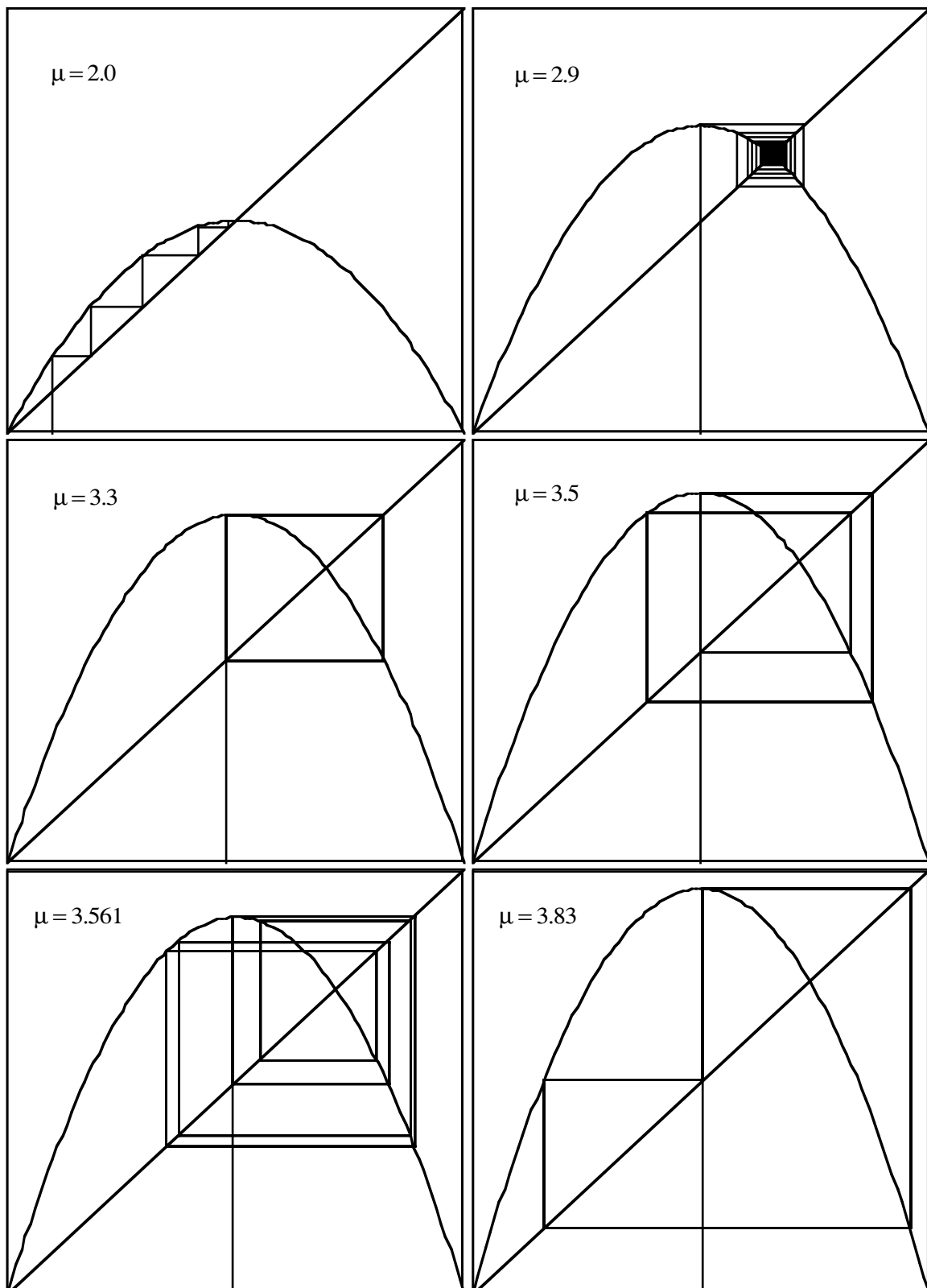


Figure 10.1 The iterates of the quadratic map for some particular values of the parameter μ . The horizontal axis is x_n and the vertical axis is x_{n+1} . For $\mu=2$ and 2.9 there is a single stable fixed point. For $\mu=3.3$ there is a stable 2-cycle; for $\mu=3.5$ a stable 4-cycle and for $\mu=3.561$ a stable 8-cycle. The value $\mu=3.83$ is in the period three window.

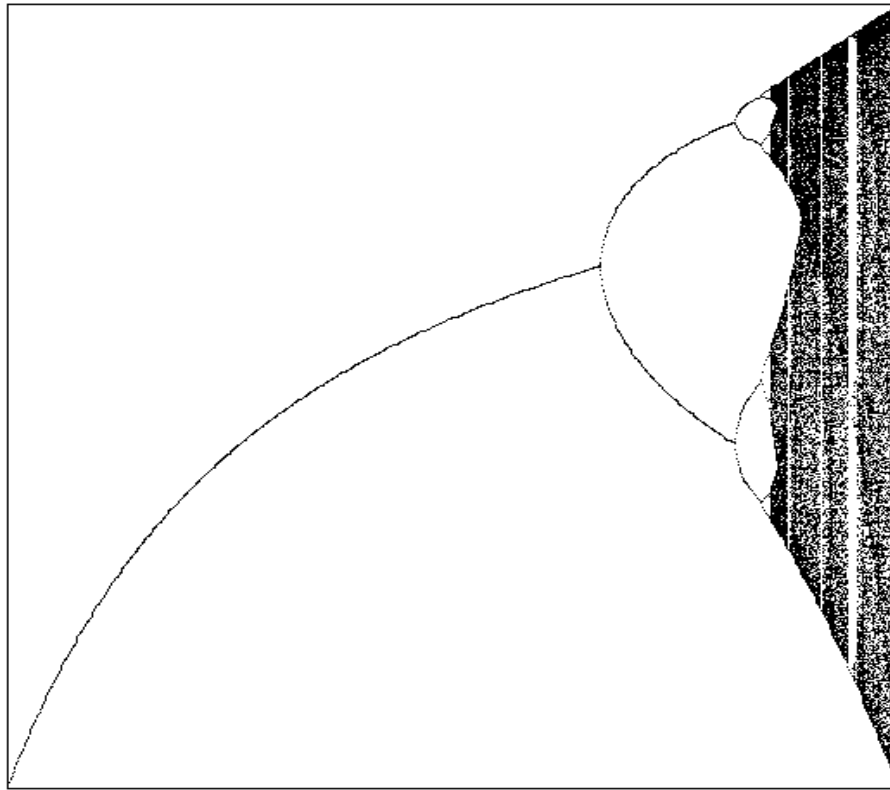


Figure 10.2 The iterates of the quadratic map as a function of the parameter μ . The horizontal axis is the parameter $1 \leq \mu \leq 4$, and the vertical axis is the iterate $0 \leq x_n \leq 1$.

The Chaotic Region $\mu_\infty < \mu < 4$

Here stable periodic and chaotic regions are densely interwoven. Chaos here is characterized by sensitive dependence on the initial value x_0 . Close to every value of μ where there is chaos, there is a value of μ which corresponds to a stable periodic orbit, that is, the mapping also displays sensitive dependence on the parameter μ . The windows of period three, five and six are examples. From the mathematical perspective the sequence of cycles in a unimodal map is completely determined by the Sarkovskii theorem (1964). If $f(x)$ has a point x which leads to a cycle of period p then it must have a point x' which leads to a q -cycle for every $q \leftarrow p$ where p and q are elements of the following sequence (here we read \leftarrow as *precedes*)

$$\begin{aligned}
 &1 \leftarrow 2 \leftarrow 4 \leftarrow 8 \leftarrow 16 \leftarrow 32 \leftarrow \dots \leftarrow 2^m \leftarrow \dots \\
 &\dots \leftarrow 2^m \cdot 9 \leftarrow 2^m \cdot 7 \leftarrow 2^m \cdot 5 \leftarrow 2^m \cdot 3 \leftarrow \dots \\
 &\dots \leftarrow 2^2 \cdot 9 \leftarrow 2^2 \cdot 7 \leftarrow 2^2 \cdot 5 \leftarrow 2^2 \cdot 3 \leftarrow \dots \\
 &\dots \leftarrow 2^1 \cdot 9 \leftarrow 2^1 \cdot 7 \leftarrow 2^1 \cdot 5 \leftarrow 2^1 \cdot 3 \leftarrow \dots \\
 &\dots \leftarrow 9 \leftarrow 7 \leftarrow 5 \leftarrow 3
 \end{aligned}$$

This theorem applies to values of x at a fixed parameter μ , but says nothing about the stability of the cycle or the range of parameter values for which it is observed.

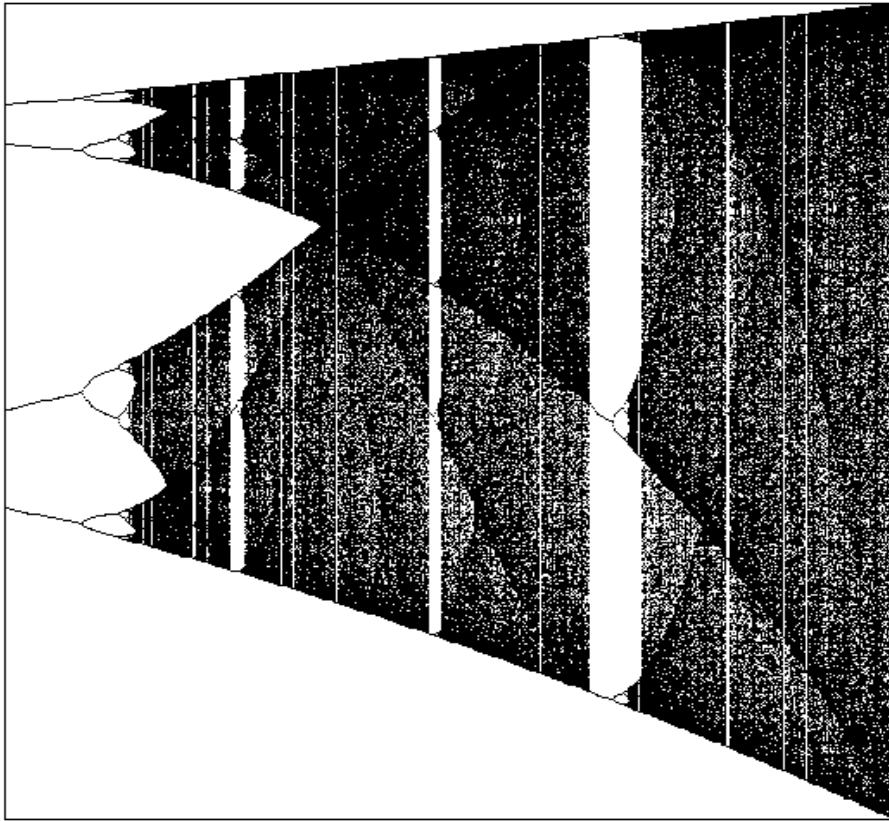


Figure 10.3 The iterates of the quadratic map as a function of the parameter μ . This is an expanded version of Figure 10.2 to include more detail in the chaotic region. The horizontal axis is the parameter $3.5 \leq \mu \leq 4$, and the vertical axis is the iterate $0 \leq x_n \leq 1$. The windows of period three (at about $\mu=3.83$), period five (at about $\mu=3.74$), and period six (at about 3.63) are clearly visible.

Region ∞ $\mu = 4$

Surprisingly for this special value of μ it is possible to solve the mapping exactly (Kadanoff, 1983). Making the substitution $x_n = (1 - \cos 2\pi\theta_n)/2$

$$\begin{aligned} x_{n+1} &= \frac{1}{2}(1 - \cos 2\pi\theta_{n+1}) = 4 \frac{(1 - \cos 2\pi\theta_n)}{2} \left[1 - \frac{(1 - \cos 2\pi\theta_n)}{2} \right] \\ &= \frac{1}{2}(1 - \cos 4\pi\theta_n) \end{aligned} \quad (10.2.4)$$

A solution is $\theta_{n+1} = 2\theta_n \bmod 1$, or $\theta_n = 2^n \theta_0 \bmod 1$. Since x_n is related to $\cos 2\pi\theta_n$ adding an integer to θ_n leads to the same value of x_n . Only the fractional part of θ_n has significance. If θ_n is written in binary (base 2) notation

$$\theta_n = 0.a_1a_2a_3a_4a_5\dots = \sum_{i=1}^{\infty} a_i 2^{-i} \quad (10.2.5)$$

then the mapping is simply shifting the decimal point one place to the right and removing the integer part of θ_{n+1} . The equivalent mapping is

$$f(0.a_1a_2a_3a_4a_5\dots) = 0.a_2a_3a_4a_5\dots \quad (10.2.6)$$

It is easy to see that any finite precision approximation to the initial starting value θ_0 consisting of N digits will lose all of its significant digits in N iterations.

If x_0 evolves to $f(x_0)$ after one iteration then the distribution $\delta(x-x_0)$ evolves to $\delta(x-f(x_0))$ after one iteration. This can be written as

$$\delta(x-f(x_0)) = \int_0^1 dy \delta(x-f(y)) \delta(y-x_0) \quad (10.2.7)$$

An arbitrary density $\rho_n(x)$ constructed from a normalized sum of (perhaps infinitely many) delta functions, satisfies an equation of the form

$$\rho_{n+1}(x) = \int_0^1 dy \delta(x-f(y)) \rho_n(y) \quad (10.2.8)$$

The invariant measure $\rho(x)$, or steady state distribution, is independent of time (or iteration number n) so

$$\rho(x) = \int_0^1 dy \delta(x-f(y)) \rho(y). \quad (10.2.9)$$

There is no unique solution to this equation as $\rho(x) = \delta(x-x^*)$ where x^* is an unstable fixed point of the map, is always a solution. However, in general there is a physically relevant solution and it corresponds to the one that is obtained numerically. This is because the set of unstable fixed points is measure zero in the interval $[0,1]$ so the probability of choosing to start a numerical calculation from an unstable fixed point x^* , and remaining on x^* , is zero due to round off and truncation errors.

In Figure 10.4 we present the invariant measure of the quadratic map in the chaotic region. The parameter value is $\mu=3.65$. The distribution contains a number of dominant peaks which are in fact fractional power law singularities.

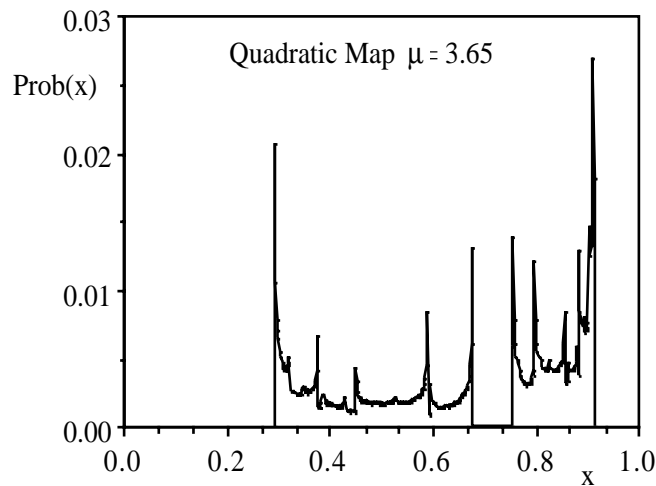


Figure 10.4 The distribution function for the iterates of the quadratic map in the chaotic region, at $\mu=3.65$. The horizontal axis is the value of the iterate, and the vertical axis is the probability. Notice the distribution of narrow peaks which dominate the probability distribution.

For the transformed mapping $\theta_{n+1} = 2\theta_n \bmod 1$, it is easy to see that the continuous loss of information about the initial starting point with each iteration of the map, means that the invariant measure as a function of θ is uniform on $[0,1]$ (that is $g(\theta)=1$). From the change of variable $x = (1 - \cos 2\pi\theta)/2$ it is easy to see that x is a function of θ , $x = q(\theta)$ (but not the reverse). If $x_1 = q(\theta_1)$, then the number of counts in the distribution function histogram bin centered at x_1 with width dx_1 , is equal to the number of counts in the bins centered at θ_1 and $1-\theta_1$ with widths $d\theta_1$. That is

$$f(x_1) = \frac{g(\theta_1) + g(1-\theta_1)}{|dx/d\theta|}. \quad (10.2.10)$$

It is then straightforward to show that the invariant measure as a function of x is given by

$$f(x) = \frac{1}{\pi} \frac{1}{\sqrt{x(1-x)}}. \quad (10.2.11)$$

In Figure 10.5 we present the invariant measure for the quadratic map at $\mu=4$. The two singularities of type $(x-x_0)^{-1/2}$ at $x_0 = 0$ and $x_0 = 1$ are clearly shown.

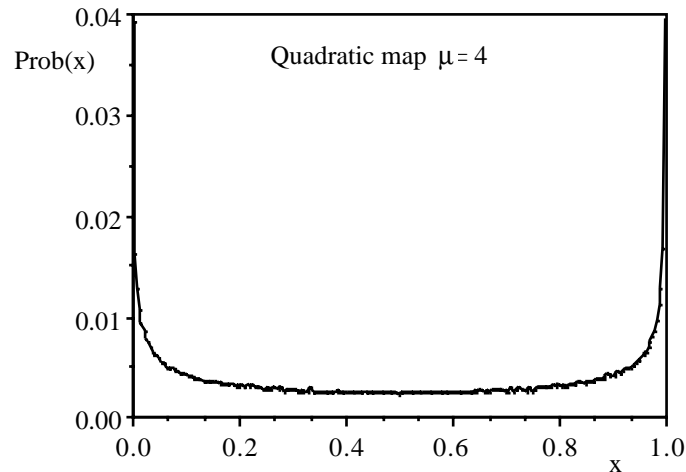


Figure 10.5 The distribution of iterates for the quadratic map at $\mu=4$. The horizontal axis is the iterate, and the vertical axis is the probability. When correctly normalized, this agrees well with equation (10.2.11).

Region ∞ $\mu > 4$

Here the maximum of $F_\mu(x)$ is greater than one. Once the iterate leaves the interval $0 < x < 1$ it does not return. The mapping $F_\mu^2(x)$ has two maxima, both of which are greater than one. If I is the interval 0 to 1, and A_1 is the region of I mapped out of I by the mapping $F_\mu(x)$, A_2 the region of I mapped out of I by $F_\mu^2(x)$, etc., then the trajectory wanders the interval defined by $I - (A_0 \cup A_1 \cup A_2 \cup \dots)$. It can be shown that this set is a Cantor set.

This example of a seemingly very simple iterative equation has very complex behaviour as a function of the parameter μ . As μ is increased the stable fixed point becomes unstable and is replaced by stable 2^n - cycles (for $n=1,2,3,\text{etc.}$), until chaotic behaviour develops at μ_∞ (about 3.5699456). For $\mu_\infty > 3.5699456$ the behaviour of the quadratic map shows sensitive dependence upon the parameter μ , with an infinite number of islands of periodic behaviour immersed in a sea of chaos. This system is not atypical, and a wide variety of nonlinear problems show this same behaviour. We will now consider a simple model from hydrodynamics which has had a dramatic impact in the practical limitations of weather forecasting.

The Lorenz Model

Consider two flat plates, separated by a liquid layer. The lower plate is heated and the fluid is assumed to be two-dimensional and incompressible. A coupled set of nonlinear field equations must be solved in order to determine the motion of the fluid between the plates (the continuity equation, the Navier-Stokes equation and the energy equation). These equations are simplified by introducing the stream function in place of the two velocity components. Saltzman (1961) and Lorenz (1963) proceed by making the field equations dimensionless and then representing the dimensionless stream function and temperature by a spatial Fourier series (with time dependent coefficients). The resulting equations obtained by Lorenz are a three parameter family of three-dimensional ordinary differential equations which have extremely complicated numerical solutions. The equations are

$$\begin{bmatrix} \dot{x} \\ \dot{y} \\ \dot{z} \end{bmatrix} = \begin{bmatrix} -\sigma(x - y) \\ (r - z)x - y \\ xy - bz \end{bmatrix} \quad (10.2.12)$$

where σ , r and b are three real positive parameters. The properties of the Lorenz equations have been reviewed by Sparrow (1982) and below we summarize the principle results.

Simple Properties:

- 1) Symmetry - The Lorenz equations are symmetric with respect to the mapping $(x, y, z) \rightarrow (-x, -y, z)$.
- 2) The z -axis is invariant. All trajectories which start on the z -axis remain there and move toward the origin. All trajectories which rotate around the z -axis do so in a clockwise direction (when viewed from above the $z=0$ plane). This can be seen from the fact that if $x = 0$, then $dx/dt > 0$ when $y > 0$, and $dx/dt < 0$ when $y < 0$.
- 3) Existence of a bounded attracting set of zero volume, that is the existence of an attractor. The divergence of the flow, is given by

$$\frac{\partial \dot{x}}{\partial x} + \frac{\partial \dot{y}}{\partial y} + \frac{\partial \dot{z}}{\partial z} = -(1 + b + \sigma). \quad (10.2.13)$$

The volume element V is contracted by the flow into a volume element $V \exp[-(1+b+\sigma)t]$ in time t . We can show that there is a bounded region E , such that every trajectory eventually enters E and remains there forever. There are many possible choices of Lyapunov function which describe the surface of the region E . One simple choice is $V = rx^2 + \sigma y^2 + \sigma(z - 2r)^2$. Differentiating with respect to time and substituting the equations of motion gives

$$\frac{dV}{dt} = -2\sigma\{rx^2 + y^2 + bz^2 - 2brz\}. \quad (10.2.14)$$

Another choice of Lyapunov function is $E = r^2x^2 + \sigma y^2 + \sigma(z - r(r-1))^2$ for $b \leq r + 1$. This shows that there exists a bounded ellipsoid, and together with the negative divergence shows that there is a bounded set of zero volume within E towards which all trajectories tend.

4) Fixed points. The Lorenz equations have three fixed points; one at the origin, the other two are at $C_1 = (-\sqrt{b(r-1)}, -\sqrt{b(r-1)}, r-1)$ and $C_2 = (\sqrt{b(r-1)}, \sqrt{b(r-1)}, r-1)$.

5) Eigenvalues for linearized flow about the origin are

$$\lambda_1 = -b$$

$$\lambda_2 = \frac{-(\sigma+1) - \sqrt{(\sigma+1)^2 - 4\sigma(1-r)}}{2}$$

$$\lambda_3 = \frac{-(\sigma+1) + \sqrt{(\sigma+1)^2 - 4\sigma(1-r)}}{2}$$

6) Stability

$0 < r < 1$

The origin is stable

$r > 1$

The origin is non-stable. Linearized flow about the origin has two negative and one positive, real eigenvalues.

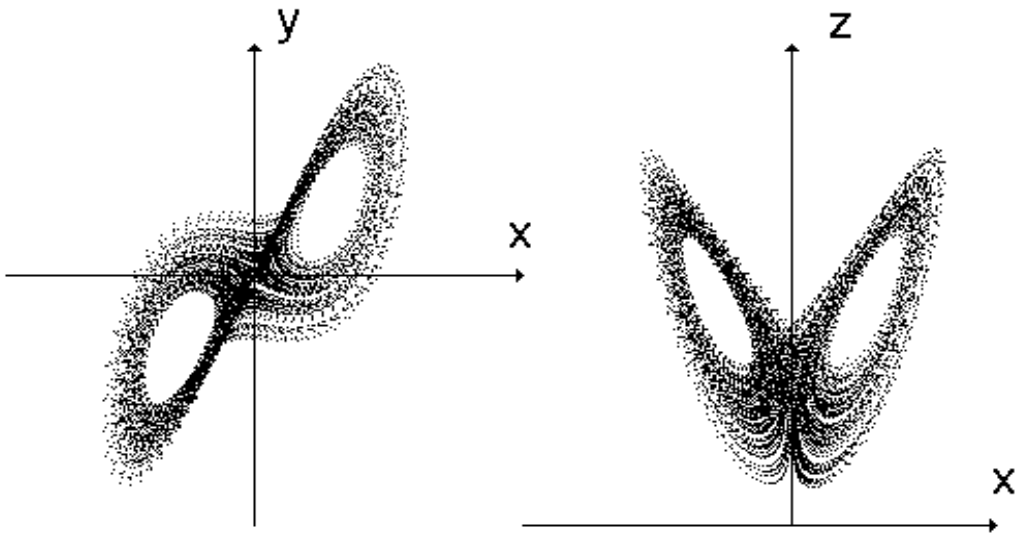
$1 < r < 470/19$

C_1 and C_2 are stable. All three eigenvalues of the linearized flow about C_1 and C_2 , have negative real part. For $r > 1.346$ ($\sigma=10$, $b=8/3$) there is a complex conjugate pair of eigenvalues.

$r > 470/19$

C_1 and C_2 are non-stable. Linearized flow about C_1 and C_2 has one negative real eigenvalue and a complex conjugate pair of eigenvalues with positive real part.

Again we have a nonlinear system which is well behaved for small values of the parameter r , but for $r > 470/19$ chaotic behaviour begins.



Lorenz Model $\sigma = 16, r = 40, b = 4$

Figure 10.6 The iterates of the Lorenz Model for a typical set of parameters which leads to chaotic behaviour. The iterates are the values obtained at the end of each 4th order Runge-Kutta step.

10.3 The Characterization of Chaos

The experimental measurement of the onset and development of chaos in dissipative physical systems is often accompanied by some arbitrariness in the choice of the measured dynamical variable. Taking fluid systems as an example, one can measure the fluid velocity, its temperature, heat flux etc. Rarely does one measure more than one variable simultaneously. Moreover, one rarely knows what is the correct, or complete, phase space in which the dissipative dynamics takes place. Thus the extraction of relevant information calls for measurement of quantities that remain invariant under a smooth change of coordinates and which can be used for a valid characterization of the dynamical system. There are two classes of these invariants. The static ones, dependent primarily on the invariant measure (the underlying distribution function for the attractor) and appear as the dimension of the attractor (either fractal, information, correlation) and as other mass exponents which have to do with various static correlation functions. The dynamic ones depend on properties of trajectories and include various entropies (topological, metric etc), the Lyapunov exponents, and moments of the fluctuations in the Lyapunov exponents. Here we present a short review of the theory of these invariants and the interrelations between them.

Studies of simple dissipative systems have shown that if we begin with a Euclidian space of initial phase positions, then as time passes, transients relax, some modes may damp out, and the point in phase space that describes the state of the system approaches an *attractor*. In this process it is common for the number of degrees of freedom to be reduced, and hence the dimension of the system is lowered. This change in dimension is a continuous process and to describe such systems we have to generalize the concept of dimension (Farmer, 1982 and Farmer, Ott and Yorke, 1983). We distinguish three intuitive notions of dimension; direction, capacity and measurement. These lead to the definition of; topological dimension (Hurewicz and Wallman, 1948), fractal dimension (Mandelbrot, 1983) and information dimension (Balatoni and Renyi, 1976). As we will see the fractal and information dimensions allow the dimension to be a continuous positive variable.

The Fractal and Information dimensions

The fractal dimension of an attractor can be defined by the following construction. Let $b(\epsilon)$ be the minimum number of balls of diameter ϵ needed to cover the attractor. The fractal dimension is defined by the limit,

$$D_F = \lim_{\epsilon \rightarrow 0} \frac{\ln b(\epsilon)}{|\ln \epsilon|}. \quad (10.3.1)$$

As the length scale ϵ is reduced, the number of balls required to cover the attractor increases. As $b(\epsilon)$ is a positive integer, its logarithm is positive. The term $\ln \epsilon$ is negative as soon as the length scale ϵ is less than one (in the appropriate units), so the dimension is a positive real quantity.

To obtain the information dimension we suppose an observer makes an isolated measurement of the coarse grained probability distribution function p_i . Coarse graining implies a length scale ϵ for the observation, and an associated number of cells $N(\epsilon)$. The discrete, or coarse grained, entropy $S(\epsilon)$ as a function of the length scale is given by

$$S(\epsilon) = - \sum_{i=1}^{N(\epsilon)} p_i \ln p_i \quad (10.3.2)$$

Notice that $S(\epsilon)$ is positive as for each i , $-p_i \ln p_i$ is positive. The information dimension D_I is then defined by

$$D_I = \lim_{\epsilon \rightarrow 0} \frac{S(\epsilon)}{|\ln \epsilon|} \quad (10.3.3)$$

This dimension is a property of any distribution function as nothing in the definition is specific to attractors, or to some underlying dynamics.

If all the $N(\epsilon)$ elements have the same probability then $S(\epsilon) = \ln N(\epsilon)$. Further if $b(\epsilon)$ is a minimal covering, then a smaller covering can be formed by removing the overlapping parts of circles so that $\ln b(\epsilon) \geq \ln N(\epsilon) = S(\epsilon)$. It is then straightforward to see that the fractal dimension is an upper bound on the information dimension. (We will generalize this result later.) From a computational point of view it is easier to tabulate the steady state distribution function and calculate D_I , rather than to attempt to identify the attractor and construct a covering to calculate D_F .

Correlation Dimension

The correlation dimension D_C introduced by Grassberger and Procaccia (1983) is a scaling relation on the correlation function $C(\epsilon)$ where

$$C(\epsilon) = \frac{1}{N^2} \sum_{i \neq j} \theta(\epsilon - |\Gamma_i - \Gamma_j|) \quad (10.3.4)$$

Here $\theta(x)$ is the Heavyside step function. $C(\epsilon)$ is the correlation integral which counts the number of pairs of points whose distance of separation $|\Gamma_i - \Gamma_j|$ is less than ϵ . The correlation dimension is

$$D_C = \lim_{\epsilon \rightarrow 0} \lim_{N \rightarrow \infty} \frac{\ln C(\epsilon)}{|\ln \epsilon|} . \quad (10.3.5)$$

It has been argued that the correlation dimension can be calculated numerically, more easily and more reliably than either the information dimension or the fractal dimension.

Generalized Dimensions

In a series of paper by Grassberger (1983), Hentschel and Procaccia (1983) Halsey et. al. (1986), and Procaccia (1985) it has been shown that the concept of dimension can be generalized further. They introduce a generating function D_q which provides an infinite spectrum of dimensions depending upon the value of q . We will show that all previous dimensions are related to special values of q . Again we divide the attractor into boxes of linear dimension ϵ , and let p_i be the probability that the trajectory on the strange attractor visits box i . By averaging powers of the p_i 's over all boxes, the generalized dimension D_q is obtained

$$D_q = - \lim_{\epsilon \rightarrow 0} \frac{1}{q-1} \frac{1}{|\ln \epsilon|} \ln \left(\sum_i p_i^q \right). \quad (10.3.6)$$

There are formal similarities between the D_q and the free energy per particle F_β in the thermodynamic limit,

$$F_\beta = - \lim_{N \rightarrow \infty} \frac{1}{\beta} \frac{1}{N} \ln \left(\sum_i (e^{-E_i})^\beta \right) \quad (10.3.7)$$

where E_i are the energy levels in the system, N is the number of particles and $\beta = (k_B T)^{-1}$ is the inverse temperature. The analogy is not a strict one as the probability of state i , is $\exp(-\beta E_i)$ rather than simply $\exp(-E_i)$ as implied above. Also the probabilities p_i are normalized, while neither $\exp(-\beta E_i)$ nor $\exp(-E_i)$ are normalized. This is crucial in statistical mechanics since if normalized probabilities are inserted into equation (10.3.7) in place of $\exp(-\beta E_i)$, the free energy F_β is trivially zero.

It straightforward to see that D_q gives each of the previously defined dimensions. For $q=0$, $p_i^q = 1$ for all values of i , so that

$$D_0 = \lim_{\epsilon \rightarrow 0} \frac{\ln \sum_{i=1}^{N(\epsilon)} 1}{|\ln \epsilon|} = \lim_{\epsilon \rightarrow 0} \frac{\ln N(\epsilon)}{|\ln \epsilon|}. \quad (10.3.8)$$

This is the fractal or Hausdorff dimension equation (10.3.1).

For $q=1$ consider the limit

$$\lim_{q \rightarrow 1} \frac{\ln \sum_i p_i^q}{q-1} = \lim_{q \rightarrow 1} \frac{\frac{d}{dq} \ln \sum_i p_i^q}{\frac{d}{dq} (q-1)} = \sum_i p_i \ln p_i = -S(\epsilon). \quad (10.3.9)$$

Substituting this limit into the expression for D_q gives

$$\lim_{q \rightarrow 1} D_q = \lim_{\varepsilon \rightarrow 0} \frac{S(\varepsilon)}{|\ln \varepsilon|} = D_1. \quad (10.3.10)$$

This is simply the information dimension. For $q=2$ it is easy to show that the generalized dimension is the correlation dimension.

The generalized dimension D_q is a non-increasing function of q . To show this we consider the generalized mean $M(t)$ of the set of positive quantities $\{a_1, \dots, a_n\}$, where p_k is the probability of observing a_k . The generalized mean is defined to be

$$M(t) = \left(\sum_{k=1}^n p_k a_k^t \right)^{1/t} \quad (10.3.11)$$

This reduces to the familiar special cases; $M(1)$ is the arithmetic mean and the limit as $t \rightarrow 0$ is the geometric mean. It is not difficult to show that if $a_k = p_k(\varepsilon)$, where the $p_k(\varepsilon)$ are a set of discrete probabilities calculated using a length scale of ε , then the generalized dimension in equation (10.3.6) is related to the generalized mean by

$$D_q = - \lim_{\varepsilon \rightarrow 0} \frac{\ln M(q-1)}{|\ln \varepsilon|}. \quad (10.3.12)$$

Using a theorem concerning generalized means, $M(t) \leq M(s)$ if $t < s$ (Hardy, Littlewood and Pólya (1934), page 26) it follows that if $s > t$ then $D_s \leq D_t$.

The Probability Distribution on the Attractor

If we consider the quadratic map for $\mu=4$, the distribution of the iterates shown in Figure 10.5, is characterized by the two singularities at $x=0$ and $x=1$. For $\mu=3.65$, the distribution of iterates, shown in Figure 10.4, has approximately ten peaks which also appear to be singularities. It is common to find a probability distribution on the attractor which consist of sets of singularities with differing fractional power law strengths. This distribution of singularities can be calculated from the generalized dimension D_q . To illustrate the connection between the generalized dimensions D_q and the singularities of the distribution function, we consider a one-dimensional system whose underlying distribution function is

$$\rho(x) = \frac{1}{2} x^{-1/2} \quad \text{for } 0 \leq x \leq 1. \quad (10.3.13)$$

First note that, despite the fact that $\rho(x)$ is singular, $\rho(x)$ is integrable on the interval $0 \leq x \leq 1$ and it is correctly normalized. The generalized dimension D_q is defined in terms of discrete probabilities so we divide the interval into bins of length ε - $[0, \varepsilon)$ is bin 0, $[\varepsilon, 2\varepsilon)$ is bin 1, etc.. The probability of bin 0 is given by

$$p_0 = \int_0^{\epsilon} dx \frac{1}{2} x^{-1/2} = \epsilon^{1/2} \quad (10.3.14)$$

and in general the probability of bin i is given by

$$p_i = \int_{x_i}^{x_i+\epsilon} dx \frac{1}{2} x^{-1/2} = (x_i+\epsilon)^{1/2} - x_i^{1/2} \quad (10.3.15)$$

where $x_i = i\epsilon$. As $(x_i+\epsilon)^{1/2}$ is analytic for $i \neq 0$, we can expand this term to obtain

$$p_i = \frac{1}{2} x_i^{-1/2} \epsilon + O(\epsilon^2) = \rho(x_i) \epsilon + O(\epsilon^2) \quad (10.3.16)$$

So for $i=0$, $p_i \sim \epsilon^{1/2}$ but for all nonzero values of i , $p_i \sim \epsilon$. To construct D_q we need to calculate

$$\sum_{i=0}^q p_i^q = p_0^q + \sum_{i \neq 0} p_i^q = \epsilon^{q/2} + \epsilon^{q-1} \sum_{i \neq 0} \rho(x_i)^q \epsilon \quad (10.3.17)$$

We can replace the last sum in this equation by an integral,

$$\sum_{i \neq 0} \rho(x_i)^q \epsilon \cong \int_{\epsilon}^1 dx \rho(x)^q = a (1 - \epsilon^{1-q/2}) \quad (10.3.18)$$

where $a = (1/2)^q (1 - q/2)^{-1}$. Combining this result with that for $i=0$ we obtain

$$\sum_i p_i^q = (1 - a) \epsilon^{q/2} + a \epsilon^{q-1} \quad (10.3.19)$$

The distribution function $\rho(x)$ in equation (10.3.13) gives rise to singularities in the discrete probabilities p_i .

If the discrete probabilities scale with exponent α , so that $p_i \sim \epsilon^{\alpha i}$ and

$$p_i^q \sim \epsilon^{\alpha q i}, \quad (10.3.20)$$

then α can take on a range of values corresponding to different regions of the underlying probability distribution. In particular, if the system is divided into pieces of size ϵ , then the number of times α takes on a value between α' and $\alpha'+d\alpha'$ will be of the form

$$d\alpha' \rho(\alpha') \varepsilon^{-f(\alpha')}, \quad (10.3.21)$$

where $f(\alpha')$ is a continuous function. The exponent $f(\alpha')$ reflects the differing dimensions of the sets whose singularity strength is α' . Thus fractal probability distributions can be modeled by interwoven set of singularities of strength α , each characterized by its own dimension $f(\alpha)$.

In order to determine the function $f(\alpha)$ for a given distribution function, we must relate it to observable properties, in particular we relate $f(\alpha)$ to the generalized dimensions D_q . As q is varied, different subsets associated with different scaling indices become dominant. Using equation (10.3.21) we obtain

$$\sum_i p_i^q = \sum_i \varepsilon_i^{\alpha q} = \int d\alpha' \rho(\alpha') \varepsilon^{-f(\alpha')} \varepsilon^{\alpha' q}. \quad (10.3.22)$$

Since ε is very small, the integral will be dominated by the value of α' which makes the exponent $q\alpha' - f(\alpha')$ smallest, provided that $\rho(\alpha')$ is nonzero. The condition for an extremum is

$$\frac{d}{d\alpha'} [q\alpha' - f(\alpha')] = 0 \quad \text{and} \quad \frac{d^2}{d\alpha'^2} [q\alpha' - f(\alpha')] > 0, \quad (10.3.23)$$

If $\alpha(q)$ is the value of α' which minimizes $q\alpha' - f(\alpha')$ then $f'(\alpha(q)) = q$ and $f''(\alpha(q)) < 0$. If we approximate the integral in equation (10.3.22) by its maximum value, and substitute this into equation (10.3.6) then

$$D_q = \frac{1}{q-1} [q\alpha(q) - f(\alpha(q))]. \quad (10.3.24)$$

so that

$$f(\alpha) = q \alpha(q) - (q-1) D_q. \quad (10.3.25)$$

Thus if we know $f(\alpha)$, and the spectrum of α values we can find D_q . Alternatively, given D_q we can find $\alpha(q)$, since $f'(\alpha) = q$ implies that

$$\alpha(q) = \frac{d}{dq} [(q-1) D_q], \quad (10.3.26)$$

and knowing $\alpha(q)$, $f(\alpha(q))$ can be obtained.

Dynamic Invariants

Grassberger and Procaccia (1983) and Eckmann and Procaccia (1986) have shown

that it is possible to define a range of scaling indices for the dynamical properties of chaotic systems. Suppose that phase space is partitioned into boxes of size ε , and that a measured trajectory $\mathbf{X}(t)$ is in the basin of attraction. The state of the system is measured at intervals of time τ . Let $p(i_1, \dots, i_n)$ be the joint probability that $X(t=\tau)$ is in box i_1 , $X(t=2\tau)$ is in box i_2, \dots , and $X(t=n\tau)$ is in box i_n . The generalized entropies K_q are defined by

$$K_q = - \lim_{\tau \rightarrow 0} \lim_{\varepsilon \rightarrow 0} \lim_{n \rightarrow \infty} \frac{1}{n\tau} \frac{1}{q-1} \ln \sum_{i_1, i_2, \dots, i_n} p^q(i_1, i_2, \dots, i_n) \quad (10.3.27)$$

where the sum is over all possible sequences i_1, \dots, i_n . As before the most interesting K_q for experimental applications are the low order ones. The limit $q \rightarrow 0$ $K_q = K$ is the Kolmogorov or metric entropy, whereas K_2 has been suggested as a useful lower bound on the metric entropy. For a regular dynamical system $K=0$, and for a random signal $K=\infty$. In general for a chaotic system K is finite, and related to the inverse predictability time and to the sum of the positive Lyapunov exponents. The Legendre transform of $(q-1)K_q$, that is $g(\Lambda)$, is the analogue of singularity structure quantities $f(\alpha)$ introduced in the last section (see Jensen, Kadanoff and Procaccia, 1987 for more details).

Lyapunov Exponents

In §3.4 we introduced the concept of Lyapunov exponents as a quantitative measure of the mixing properties of a system. Here we will develop these ideas further, but first we review the methods which can be used to calculate the Lyapunov exponents. The standard method of calculating Lyapunov exponents for dynamical systems is due to Benettin et. al. (1976) and Shimada and Hagashima (1979). They linearize the equations of motion and study the time evolution of a set of orthogonal vectors. To avoid problems with rapidly growing vector lengths they periodically renormalize the vectors using a Gram-Schmidt procedure. This allows one vector to follow the fastest growing direction in phase space, and the second to follow the next fastest direction, while remaining orthogonal first vector, etc. The Lyapunov exponents are given by the average rates of growth of each of the vectors.

A new method of calculating Lyapunov exponents has been developed by Hoover and Posch (1985) and extended to multiple exponents by Morriss (1988) and Posch and Hoover (1988). It uses Gauss' principle of least constraint to fix the length of each tangent vector, and to maintain the orthogonality of the set of tangent vectors. The two extensions of the method differ in the vector character of the constraint forces - the Posch-Hoover method uses orthogonal forces, while the Morriss method uses non-orthogonal constraint forces. In earlier chapters we have used Gauss' principle to change from one ensemble to another. This application of Gauss' principle to the calculation of Lyapunov exponents exactly parallels this situation. In the Benettin method one monitors the divergence of a pair of trajectories, with periodic rescaling. In the Gaussian scheme we monitor the *force* required to keep two trajectories a fixed distance apart in phase space.

Lyapunov Dimension

The rate of exponential growth of a vector $\delta x(t)$ is given by the largest Lyapunov

exponent. The rate of growth of a surface element $\delta\sigma(t)=\delta x_1(t)\times\delta x_2(t)$ is given by the sum of the two largest Lyapunov exponents. In general the exponential rate of growth of a k-volume element is determined by the sum of the largest k Lyapunov exponents $\lambda_1+\dots+\lambda_k$. This sum may be positive implying growth of the k-volume element, or negative implying shrinkage of the k-volume element.

A calculation of the Lyapunov spectrum gives as many Lyapunov exponents as phase space dimensions. All of the previous characterizations of chaos that we have considered, have led to a single scalar measure of the dimension of the attractor. From a knowledge of the complete spectrum of Lyapunov exponents Kaplan and Yorke (1979) have conjectured that the effective dimension of an attractor is given by that value of k for which the k-volume element neither grows nor decays. This requires some generalization of the idea of a k-dimensional volume element as the result is almost always non-integer. The Kaplan and Yorke conjecture is that the Lyapunov dimension can be calculated from

$$D_L^{KY} = n + \frac{\sum_{i=1}^n \lambda_i}{|\lambda_{n+1}|} \quad (10.3.28)$$

where n is the largest integer for which $\sum_{i=1}^n \lambda_i > 0$.

Essentially the Kaplan-Yorke conjecture corresponds to plotting the sum of Lyapunov exponents $\sum_{i=1}^n \lambda_i$ versus n , and the dimension is estimated by finding where the curve intercepts the n -axis by linear interpolation.

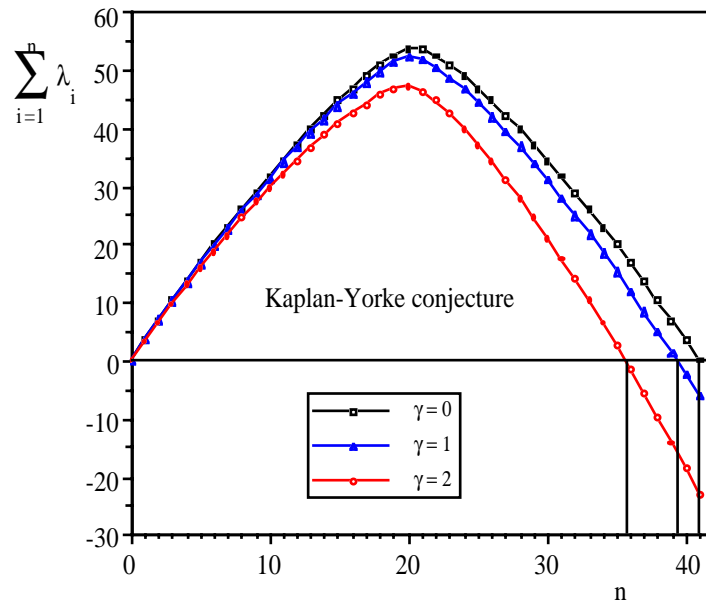



Figure 10.7 We show the sum of the largest n exponents, plotted as a function of n , for three-dimensional 8-particle Couette flow at three different shear rates $\gamma = 0, 1$, and 2 . The Kaplan-Yorke dimension is the n -axis intercept.

There is a second postulated relation between Lyapunov exponents and dimension due to Mori (1980).

$$D_L^M = m_0 + m^+ \left(1 + \frac{|\lambda^+|}{|\lambda^-|} \right) \quad (10.3.29)$$

where m_0 and m^+ are the number of zero and positive exponents respectively, and λ^\pm is the mean value of the positive or negative exponents (depending upon the superscript). Farmer (1982) gives a modified form of the Mori dimension which is found to give integer dimensions for systems of an infinite number of degrees of freedom. 

10.4 Chaos in Planar Couette Flow

We have seen in §10.2 that in apparently simple dynamical systems such as the quadratic map and the Lorenz model, a single trajectory or sequence of iterates can have quite unusual behavior. In §10.3 we introduced a number of techniques to characterize the dynamical behavior of a system with a strange attractor. Here we will apply those techniques to the SLLOD planar Couette flow algorithm that was introduced in Chapter 6. The first difficulty is that to apply the various techniques that determine the dimension of an attractor, the dimension of the initial phase space must be small enough to make the numerical calculations feasible. To calculate the static dimensions D_q we need to calculate the discrete probability distribution function. To do this we divide phase space up into boxes of size ϵ . The number of boxes needed varies as $(1/\epsilon)^{6N}$, for a $6N$ dimensional phase space. Such a calculation quickly becomes impractical as the phase space dimension increases. A typical statistical mechanical system has a phase space of $2dN$ dimensions (where d is the dimension of the translational coordinate space of a single particle) so clearly N must be small, but also N must be large enough to give nontrivial behavior. Surprisingly enough both of these considerations can be satisfied with $d=2$ and $N \geq 2$ (Ladd and Hoover, 1985, Morriss et.al., 1985,1986).

The SLLOD equations of motion for Gaussian thermostatted planar Couette flow are;

$$\dot{\mathbf{q}}_i = \frac{\mathbf{p}_i}{m} + \mathbf{i} \gamma y_i$$

$$\dot{\mathbf{p}}_i = \mathbf{F}_i - \mathbf{i} \gamma p_{yi} - \alpha \mathbf{p}_i \quad (10.4.1)$$

$$\alpha = \frac{\sum_{i=1}^N (\mathbf{F}_i \cdot \mathbf{p}_i - \gamma p_{xi} p_{yi})}{\sum_{i=1}^N \mathbf{p}_i^2} \quad (10.4.2)$$

\mathbf{i} is the unit vector in the x-direction, and γ is the strain rate. The dissipative flux $J(\Gamma)$ due to the applied field is found from the adiabatic time derivative of the internal energy H_0 . Here $J(\Gamma)$ is the shear stress $P_{xy}(\Gamma)$ times the volume V ;

$$P_{xy}(\Gamma) V = \sum_{i=1}^N \left(\frac{p_{xi} p_{yi}}{m} + y_i F_{xi} \right) \quad (10.4.3)$$

and the shear rate dependent viscosity $\eta(\gamma)$ is related to the shear stress in the usual way $\eta(\gamma) \gamma = -\langle P_{xy} \rangle$.

If we consider a two-dimensional, two-body, planar Couette flow system we find that

the total phase space has eight degrees of freedom - $\{x_1, y_1, x_2, y_2, p_{x1}, p_{y1}, p_{x2}, p_{y2}\}$. We then construct an infinite system made up of periodic replications of the central two-particle square, using the usual *sliding brick* periodic boundary conditions (see §6.3). We choose an origin for the coordinate axis where $\sum_i \mathbf{p}_i = 0$ and $\sum_i y_i = 0$. In this case both the centre of mass and the total momentum are constants of the motion. If the total kinetic energy (kinetic temperature) is also fixed, the accessible phase space has three dimensions. A convenient choice for these three variables is; the relative separation of the two particles $(x_{12}, y_{12}) = (x_2 - x_1, y_2 - y_1)$, and the direction of the momentum vector of particle one (p_{x1}, p_{y1}) with respect to the x-axis, which we call θ . The magnitude of the momentum is fixed by the total kinetic energy constraint and the fact that $\mathbf{p}_1 + \mathbf{p}_2 = 0$. For $N > 2$ we find the total phase space reduces from $4N$ degrees of freedom to $4N - 5$, when the fixed centre of mass, fixed linear momentum and the constant value of kinetic energy are taken into account. The sliding brick periodic boundary conditions in the Couette flow algorithm induce an explicit time dependence into the equations of motion for Couette flow. This is most easily seen by removing the potential cutoff. The force on particle i due to particle j is then given by a lattice sum where the positions of the lattice points are explicit functions of time. The equations of motion are then nonautonomous and hence do not have a zero Lyapunov exponent. These $4N - 5$ equations can be transformed into $4N - 4$ autonomous equations by the introduction of a trivial extra variable whose time derivative is the relative velocity of the lattice points one layer above the central cell. In this form there is a zero Lyapunov exponent associated with this extra variable (see Haken, 1983). Here we work with the $4N - 5$ nonautonomous equations of motion and we ignore this extra zero Lyapunov exponent.

Information dimension

The first evidence for the existence of a strange attractor in the phase space of the two-dimensional, two-body planar Couette flow system was obtained by Morriss (1987). He showed numerically that the information dimension of two-body planar Couette flow is a decreasing function of the strain rate, dropping steadily from three towards a value near two, before dropping dramatically at a critical value of the strain rate to become asymptotic to one. These results are for the WCA potential (equation 6.1.5) at a reduced temperature of 1 and a reduced density of 0.4. The sudden change in dimension, from a little greater than two to near one, is associated with the onset of the *string-phase* for this system (see §6.4). A change in effective dimensionality for shearing systems of 896 particles, under large shear rates, has been observed. In this case the vector separation between two atoms $\mathbf{r}_{ij} = (x_{ij}, y_{ij})$ has components whose sign is independent of time. This arises because within *strings* the atoms are ordered, and the strings themselves once formed remain forever intact, (and in the same order). It has been shown that the string phase is an artifact of the definition of the temperature with respect to an *assumed* streaming velocity profile (§6.4), so it is likely that this decrease in dimensionality is pathological, and not associated with the attractor which is found at intermediate strain rates.

Generalized Dimensions

Morriss (1989) has calculated the generalized dimension D_q and the spectrum of singularities $f(\alpha)$ for the steady state phase space distribution function of two dimensional two-body planar Couette flow using the WCA potential at a reduced temperature of 1 and a reduced density of 0.4. This system is identical to that considered in the information dimension calculations referred to above. The maximum resolution of the distribution function was 3×2^6 bins in each of the three degrees of freedom, leading to more accurate results than the previous information dimension calculations. He found that at equilibrium the discrete probabilities $p_i(\epsilon)$ scale with the dimension of the initial phase space. Away from equilibrium the $p_i(\epsilon)$ scale with a range of indices, extending from the full accessible phase space dimension to a lower limit which is controlled by the value of the shear rate γ .

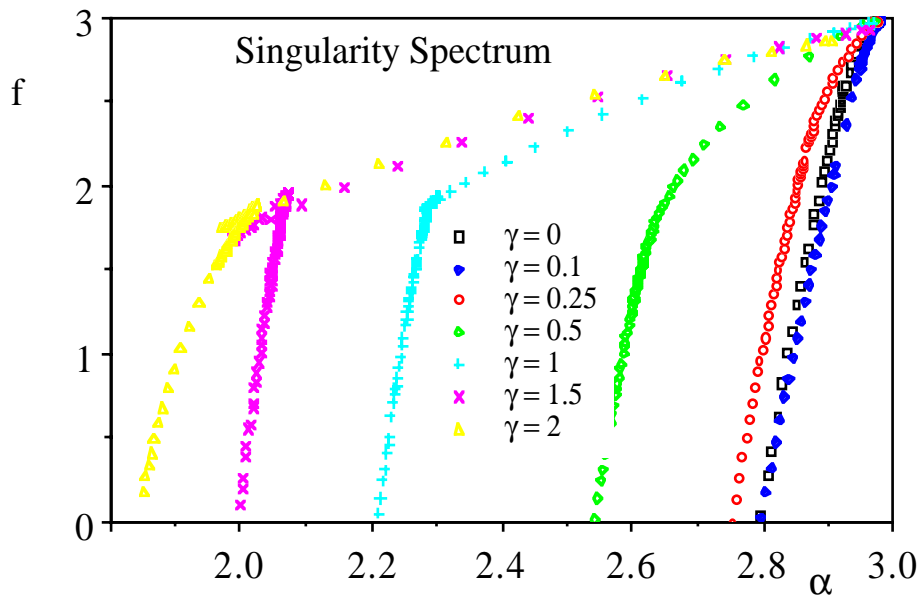


Figure 10.8 The spectrum of phase space singularities for two dimensional 2 particle planar Couette flow at $T^*=1$ and $\rho^*=0.4$ as a function of γ . The function $f(\alpha)$ is the dimension of the set of points on the attractor that scale with exponent α . The range of singularities extends from 3 to α_{\min} where the value of α_{\min} decreases with increasing strain rate.

In Figure 10.8 we present the singularity distribution $f(\alpha)$ for a number of values of the strain rate γ . The results near $\gamma=0$ depend significantly on the values of grid size used, and could be improved by considering finer meshes (the minimum grid size is limited by computer memory size). At higher values of γ (say $\gamma=1$) the values of $f(\alpha)$ above the shoulder in Figure 10.8, are insensitive to grid size. However, the position of the shoulder does change with grid size. In the limit $q \rightarrow \infty$, the value of D_q and hence the value of $\alpha = \alpha_{\min}$ for which $f(\alpha) \rightarrow 0$, is controlled by the scaling of the most probable p_i in the histogram p_{\max} . It is easy to identify p_{\max} and determine its scaling as an independent check on the value of α_{\min} . Just as large positive values of q weight the most probable p_i most strongly, large negative values of q weight the least probable p_i most strongly. The accuracy with which the least probable p_i can be determined limits the minimum

value of q for which the calculation of D_q is accurate. This is reflected in poor values of D_q for $q \leq 0.5$, and we believe is a contributing factor in obtaining inconsistent values of the fractal dimension D_0 .

We interpret the results shown in Figure 10.8 as follows. The value of $f(\alpha)$ is the dimension of the set of points on the attractor which scale as ϵ^α in the discrete phase space distribution function $\{p_i\}$. For this system it implies singularities of the form $|\Gamma - \Gamma_0|^{\alpha-3}$ in the underlying (continuous) phase space distribution function $f(\Gamma, \gamma)$. At equilibrium most p_i 's scale as ϵ^3 , with a very narrow spread of lower α values. Indeed with finer grid sizes this distribution may narrow still further. Away from equilibrium two effects are clearly discernible. First the dimension of the set of p_i 's which scale as ϵ^3 drops with increasing γ . Second the distribution of values of α increases downwards with the lower limit α_{\min} controlled by the value of γ . This distribution is monotonic with the appearance of a shoulder at an intermediate value of α .

Having calculated the full phase space distribution function on a resolution ϵ we can investigate the behavior of the various reduced distributions, for example we may consider the coordinate space distribution function $f_2(r, \phi)$, or the distribution of the momentum angle θ . Each of these reduced distributions is obtained by integrating (or summing) over the redundant coordinates or momenta. Perhaps the most interesting of these reduced distribution functions is the coordinate space distribution $f_2(x_{12}, y_{12})$, shown in Figure 10.9.

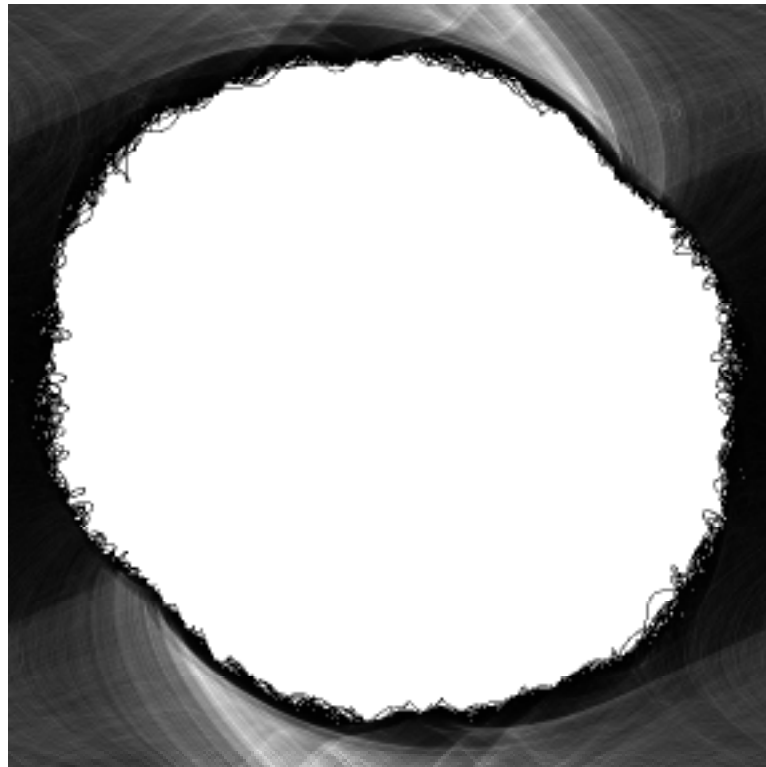


Figure 10.9 The coordinate space distribution function for the relative position coordinate (x_{12}, y_{12}) at $\gamma=1.25$. The centre of the plot is the position of particle 1 (x_1, y_1) , that is $x_{12}=y_{12}=0$. Notice that there is a preference for collisions to occur in the top right-hand side and lower left-hand side, and a significant depletion of counts near $x_{12}=0$. $\rho^*=0.4, e^*=0.25$.

If the underlying continuous distribution function has a singularity of the form $|\mathbf{\Gamma}-\mathbf{\Gamma}_0|^{\alpha-3}$, then f_2 can have singularities of the form $|\mathbf{\Gamma}-\mathbf{\Gamma}_0|^{\alpha-2}$. However, if $2 \leq \alpha \leq 3$ then these points are no longer singularities, and the reduced distribution f_2 has a different character to the full phase space distribution. If the exponent $\alpha-2$ is positive, then f_2 is zero at $\mathbf{\Gamma}_0$ and the discrete probability $p_i(\epsilon)$ which includes $\mathbf{\Gamma}_0$ will scale as ϵ^2 , whereas if $\alpha-2$ is negative then f_2 is singular.

In this study **all** the two variable distribution functions, although being highly structured in many cases, did not show any evidence of singularity sets of non-zero measure. This observation has important ramifications for the Green entropy which we will meet in §10.5.

Lyapunov Exponents

The complete set of Lyapunov exponents for two and three-dimensional planar Couette flow have been calculated for 2,4 and 8 particle systems by Morriss (1988,1989). For the two particle system the Lyapunov dimension D_L has been calculated using both the Mori and Kaplan-Yorke conjectures (equations 10.3.31 and 10.3.32). This requires the complete set of Lyapunov exponents (that is 3 exponents for $N=2$) and has the advantage over static dimensions that no subsequent extrapolation procedure is needed. The following table contains the results for the two-body, two-dimensional Couette flow system at the same state point as that used in the information and generalized dimension calculations.

For both the Kaplan-Yorke and Mori forms, the Lyapunov dimension is found to be a decreasing function of the shear rate. This is consistent with the contraction of phase space dimension that we have already seen from the numerical evaluated static dimensions D_q . It confirms that the nonequilibrium distribution function is a fractal attractor whose dimension is less than that of the equilibrium phase space. When the shear rate γ is zero, both methods of calculating the Lyapunov dimension agree. However, as soon as the shear rate changes from zero, differences appear. In the Kaplan-Yorke formula (equation 10.3.31), the value of n is 2 from $\gamma = 0$, until the magnitude of λ_2 exceeds that of λ_1 (somewhere between $\gamma = 2$ and 2.5). This means that $2 < D_{LY} < 3$ in this range. For $\gamma > 2$, $1 < D_{LY} < 2$ as long as λ_1 remains positive. The value of λ_3 is irrelevant as soon as $|\lambda_2| > \lambda_1$. Then as λ_1 becomes negative the dimension is equal to zero. The Kaplan-Yorke formula can never give fractional values between zero and one. In the Mori formula the value of λ_3 always contributes to the dimension, and its large negative value tends to dominate the denominator, reducing D_L^M . The transition from $D_L^M > 2$ to $D_L^M < 2$ is somewhere between $\gamma = 1$ and 1.5. Indeed the Mori dimension is systematically less than the Kaplan-Yorke dimension.

Table 10.1: Lyapunov Exponents for $N = 2$

γ	Lyapunov Exponents for $N = 2$			Dimension	
	λ_1	λ_2	λ_3	D_L^{KY}	D_L^M
0	2.047(2)	0.002(2)	-2.043(2)	3.003	3.00
0.25	2.063(3)	-0.046(2)	-2.1192(3)	2.952	2.90
0.5	1.995(3)	-0.187(4)	-2.242(3)	2.81	2.64
0.75	1.922(4)	-0.388(3)	-2.442(3)	2.62	2.36
1.0	1.849(5)	-0.63(1)	-2.74(1)	2.445	2.10
1.25	1.807(4)	-0.873(5)	-3.17(1)	2.295	1.89
1.5	1.800(5)	-1.121(2)	-4.12(5)	2.14	1.68
1.75	1.733(4)	-1.424(3)	-5.63(6)	2.058	1.49
2.0	1.649(9)	-1.54(1)	-7.36(8)	2.015	1.37
2.25	1.575(3)	-1.60(1)	-9.25(9)	1.981	1.29
2.5	1.61(2)	-2.14(1)	-11.5(1)	1.75	1.24
2.75	0.2616(8)	-2.12(1)	-19.84(3)	1.123	1.02
3.0	0.678(5)	-2.69(1)	-19.85(2)	1.252	1.06
3.5	-0.111(4)	-2.62(1)	-17.49(4)	0	0
4.0	0.427(4)	-4.25(1)	-14.43(5)	1.10	1.05
4.5	-0.674(5)	-2.96(1)	-10.78(3)	0	0
5.0	-0.132(2)	-1.97(1)	-8.152(3)	0	0

In Table 10.2 we compare the values of D_q for 2 particle two-dimensional planar Couette flow for several values of q , with the Kaplan-Yorke Lyapunov dimension for this system obtained from the full spectrum of Lyapunov exponents. Of the two routes to the Lyapunov dimension the Kaplan-Yorke method agrees best with the information dimension results of Table 10.2, whereas the Mori method does not. In particular the Kaplan-Yorke method and the information dimension both give a change from values greater than two, to values less than two at about $\gamma = 2.5$. There are a number of points to note about the results in this table. First, it can be shown that D_1 is a lower bound for D_0 , however the numerical results for D_0 and D_1 are inconsistent with this requirement as $D_0 < D_1$. As we remarked previously, the results for D_q when $q < 0.5$ are poor. It has been argued that the fractal (Hausdorff) dimension and Kaplan-Yorke Lyapunov dimension should yield the same result, at least for homogeneous attractors. In this work we find that D_L^{KY} is significantly lower than D_1 (which is itself a lower bound on D_0) for all values of the strain rate. Indeed D_L^{KY} is approximately equal to D_q , where q somewhat greater than 3.

γ	Generalized Dimensions				
	D_0	D_1	D_2	D_3	D_{LK}
0.0	2.90(1)	2.98(2)	2.98(2)	2.98(2)	3.003
0.1	2.91	2.98	2.98	2.98	-
0.25	2.91	2.98	2.98	2.97	2.95
0.5	2.91	2.97	2.95	2.91	2.81
1.0	2.89(1)	2.90(3)	2.67(3)	2.49(3)	2.445
1.5	2.87	2.75	2.290	2.15	2.14
2.0	2.80(3)	2.65(3)	2.20(2)	2.10(3)	2.015

It is possible to calculate the Lyapunov exponents of systems with more than two particles, whereas extending the distribution function histogramming algorithms for the information dimension or generalized dimension is much more difficult. The full Lyapunov spectrum has been calculated for 4 and 8 particle planar Couette flow systems in both two and three dimensions.

In Figure 10.10 we show the Lyapunov spectra for the 4 particle system at $\rho=0.4$ for a range of values of the shear rate. For the equilibrium spectrum ($\gamma=0$) one exponent is zero, while the others occur in Smale pairs $\{\lambda_{-i}, \lambda_{+i}\}$, where $\lambda_{-i} = -\lambda_{+i}$. This symmetry is a consequence of the time reversibility of the equations of motion and the conservation of phase space volume from the Liouville theorem. For the two-dimensional system the exponents appear to be essentially linear in exponent number, but a linear fit to the positive exponents is not consistent with an exponent of zero for exponent number zero. As the external field is increased systematic changes in the Lyapunov spectrum occur.


The positive branch decreases, with the smallest positive exponent decreasing most. The largest positive exponent seems almost independent of the external field. We expect that the most vigorous *mixing* in phase space, which is controlled by the positive exponents, is first a function of the curvature of the particles themselves (the higher the curvature, the more defocusing is each collision), and second depends on the collision frequency (and hence the density). It could be argued that the insensitivity of the largest exponent is associated with only a small change in collision frequency with strain rate, at this density. The zero exponent becomes more negative with increasing field, as does the negative branch of the Lyapunov spectrum. The change in the negative branch is larger than the change in the positive branch. The change in the sum of each exponent pair is the same, that is $\lambda_{-i} + \lambda_{+i} = c$, where c is constant independent of i and related directly to the dissipation. The change in the exponent which is zero at equilibrium is $1/2c$. 

Figure 1

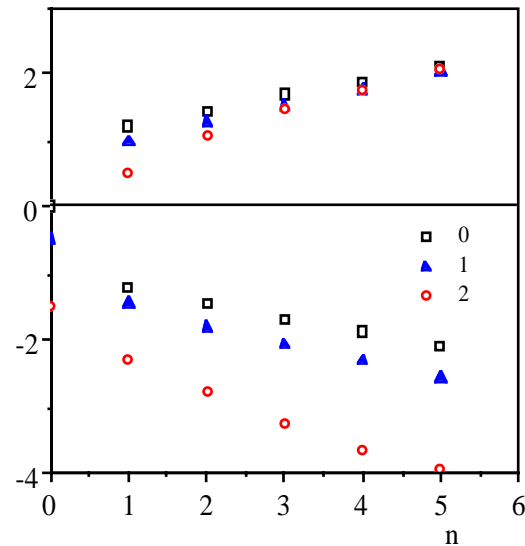


Figure 10.10 The Lyapunov spectra for two-dimensional 4 particle planar Couette flow at $T^*=1$ and $\rho^*=0.4$. The open squares are for $\gamma=0$, the filled triangles are for $\gamma=1$ and the open circles are for $\gamma=2$. The Lyapunov spectra shifts downwards with increasing strain rate with the largest exponent shifting least. The sum of the exponents is zero at equilibrium and become more negative with increasing strain rate.

The idea of being able to characterize the Lyapunov spectrum without having to calculate all of the exponents is very attractive, as the computation time for the Gaussian constraint method depends on the fourth power of the number of particles N . We decided to compare the Lyapunov spectra as a function of system size, at the same state point. It is well known that the bulk properties will have some system size dependence, but the trends as a function of density and temperature should be reliable. In Figure 10.11 we present the Lyapunov spectra for an equilibrium system at $\rho=0.4$, for a range of system sizes $N=2, 4$ and 8 . Each spectra is scaled so that the largest positive and negative exponents have the same exponent number regardless of system size. These results look very encouraging as the spectra of all three systems are very similar. The linear fit to the positive branch for $N=4$ and $N=8$ have slightly different slopes but the qualitative features are the same.

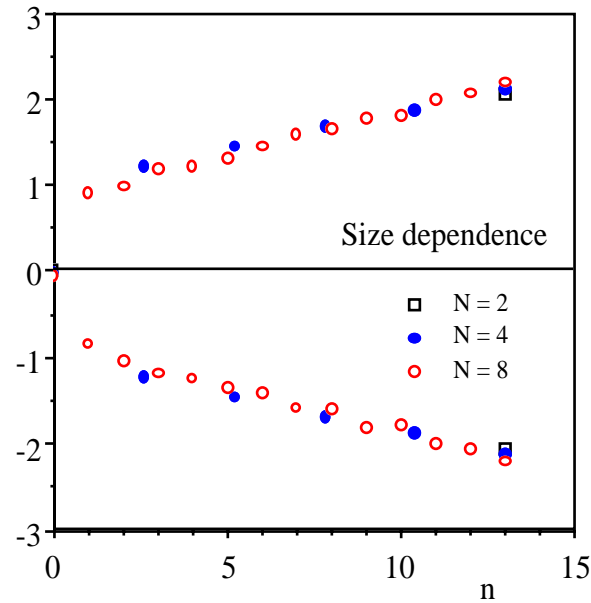


Figure 10.11 The Lyapunov spectra for two-dimensional 2,4 and 8 particle equilibrium simulations at $T^*=1$ and $\rho^*=0.4$. The spectra are scaled so that the largest positive exponent occurs at the same exponent number regardless of system size. The open squares are for $N=2$, the filled circles for $N=4$ and the open circles for $N=8$.

In Figure 10.12 we present the Lyapunov spectra for a strain rate of $\gamma=1.0$ at $\rho=0.4$, for system sizes of $N=2, 4$ and 8 . This shows that there is also a close correspondence between the results at different system sizes away from equilibrium.

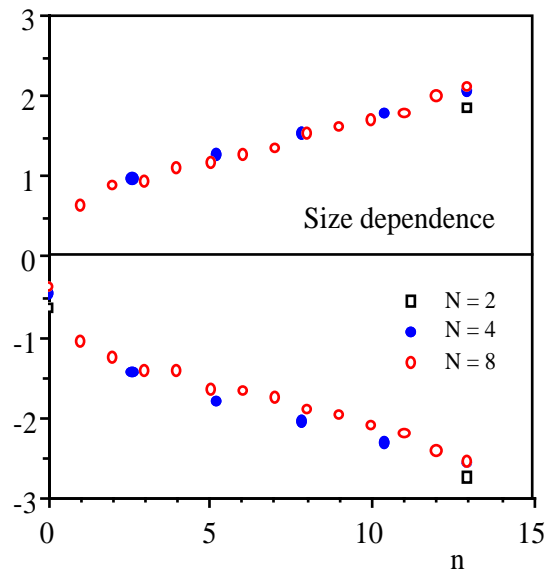


Figure 10.12 The Lyapunov spectra for two-dimensional 2, 4 and 8 particle planar Couette flow at $T^*=1$, $\rho^*=0.4$, and $\gamma=1.0$. The spectra are scaled so that the largest positive exponent occurs at the same exponent number regardless of system size. The open squares are for $N=2$, the filled circles for $N=4$ and the open circles for $N=8$. The open squares are for $N=2$, the filled circles for $N=4$ and the open circles for $N=8$.

In Figure 10.13 we show the Lyapunov dimension of the planar Couette flow system at $\rho=0.4$ as a function of strain rate, for a range of system sizes. For each system size the Lyapunov dimension is scaled by the equilibrium value, so that the plotted results represent the proportional reduction in dimension. The qualitative trends are the same. There is a decrease in dimension with increasing strain rate. The proportional change in dimension is greatest for the two particle system and smallest for the eight particle system, whereas the absolute changes are in the opposite order.

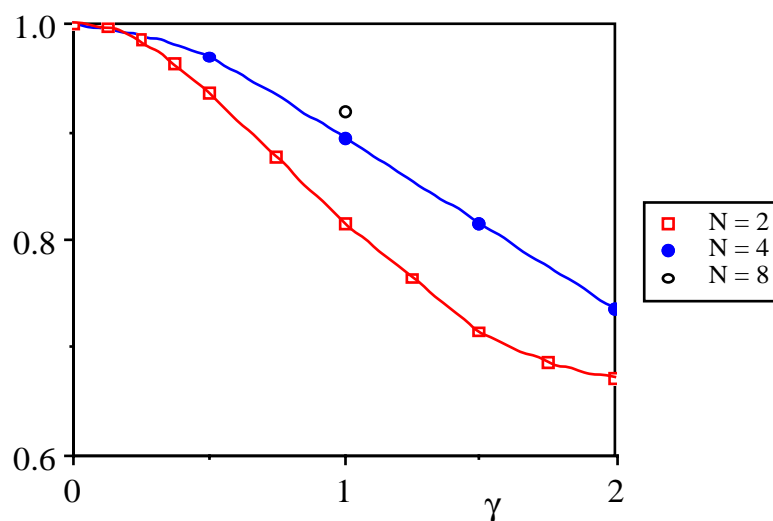


Figure 10.13 The Lyapunov dimension for two-dimensional 2, 4 and 8-particle Couette flow at $T^*=1$, $\rho^*=0.4$, as a function of strain rate. The values of dimension are scaled with respect to the equilibrium dimension so that the y-axis represents the proportional change in

dimension. The open squares are for $N=2$, the filled circles for $N=4$ and the open circles for $N=8$.

In summary, the results confirm the dimensional contraction observed previously in two body, two-dimensional planar Couette flow simulations. The initial phase space dimension of $D=2dN-2d-1$, contracts with increasing external field, and the distribution function is only nonzero on a fractal attractor of dimension less than $2dN-2d-1$. Although the results for these systems differ in detail from the generalized dimension results, the observation of significant dimensional contraction is universal. An approach which may help reduce the magnitude of the numerical calculations is the observation that the qualitative features of the spectra are essentially independent of system size.


If we consider the volume element V_{2dN} where $2dN$ is the phase space dimension of the initial system (d is the spatial dimension and N is the number of particles), then we have that the phase space compression factor gives the rate of change of phase space volume (see equation 3.4.19), so that the average of the divergence is equal to the sum of the Lyapunov exponents. A careful calculation of the divergence for the SLLOD algorithm, taking into account the precise number of degrees of freedom gives

$$\sum_{i=1}^{2dN-2d-1} \lambda_i = -(dN-d-1)\alpha + \frac{\gamma P_{xy}^K V}{(dN-d-1) kT} \quad (10.4.4)$$

where P_{xy}^K is the kinetic contribution to the shear stress and V is the volume. The term involving P_{xy}^K is order one whereas the first term is order N , so for many particle systems the second term can be ignored. For the systems considered here both terms must be included. This is a valuable consistency check on the accuracy of the numerical calculation of Lyapunov exponents.

We have now identified two effects associated with the phase space distribution functions of nonequilibrium systems; the first was dimensional contraction, and the second is a range of sets of fractional power law singularities. The two results are consistent in the sense that as each distribution function is normalized, the loss of probability due to dimensional contraction, is compensated for by the appearance of singularities in the distribution function.

Studies of two and three-dimensional colour diffusion systems by Posch and Hoover (1988) have produced an impressive calculation - the full Lyapunov spectrum for a three dimensional system of 32 repulsive Lennard-Jones atoms (185 Lyapunov exponents) - as well as results for the same system with 8 atoms. Lyapunov spectra are insensitive to ensemble, both at and away from equilibrium. All indications are that nonequilibrium systems are also insensitive to the details of the ensemble or thermostating mechanism. On the other hand boundary effects do have a significant influence on the shape of spectra for small system. In particular, the homogeneous algorithms for shear flow (such as SLLOD) give different Lyapunov exponents to boundary reservoir methods (Posch and Hoover, 1989).

As small NEMD simulations of planar Couette flow and colour diffusion are dominated by a fractal attractor whose dimension is determined by the strength of the applied field, this behaviour can be expected for all nonequilibrium steady state simulations. The existence of a fractal attractor is a vital clue to understanding the nonequilibrium entropy, but as yet we only have information concerning the rate of approach of a trajectory to the attractor, and measures of its effective dimension. We know a good deal about the structure of the attractor, and the singularities of the the nonequilibrium distribution function. Some recent work in the study of dynamical systems (Takahashi and Oono, 1984) shows that modeling chaotic behaviour with statistical mechanical analogues is a useful approach however, but to date the approach parallels irreversible thermodynamics with a continuous production of entropy. For a theory of nonequilibrium steady states, we need to be able to calculate an entropy **shift** from equilibrium to the steady state which is finite. The appearance of an attractor, and the relative stability of *entropy producing trajectories* provides a plausible explanation for the observation of irreversibility and a mechanism for the resolution of Lösschmidt's paradox (Holian, Hoover and Posch, 1987). 

It is interesting to make a connection between the results given here and the numerical calculations based on the Kawasaki distribution function. In §7.7 we described some very recent numerical studies of the Kawasaki form for the full nonlinear response of an equilibrium system subject to the sudden application of a fixed shear rate. From a theoretical point of view there are two points of interest in this stress growth experiment. First, is the renormalized Kawasaki shear stress equal to that observed directly? Second, how does the Kawasaki normalization behave as a function of time? The results show that the renormalized Kawasaki shear stress is in quite good agreement with the direct result, and that the Kawasaki normalization which is one initially, decreases with time. The results obtained here for the 2-body system suggest that the Kawasaki distribution function may have singularities which compensate for the observed decrease in both the individual probabilities and the normalization, and that these singularities are not adequately represented in the phase space sampling used.

Equation (10.1.4) implies that if we consider a comoving phase space volume element containing a fixed number of trajectories, then the local density of phase space increases indefinitely because the associated Lagrangian volume is constantly decreasing (because the sum of the Lyapunov exponents is negative). Since the contraction of the accessible phase space is *continuous* there is in a sense, no possibility of generating a steady state distribution function. Computed from the ostensible phase space the volume of accessible phase space shrinks at a constant rate becoming zero at infinite time. A steady state is in fact characterized by a constant rate of decrease in the relative volume occupied by accessible phase space. This is in spite of the fact that in a steady state averages of phase variables are constant. This apparent contradiction can be understood by considering the following example.

Suppose we consider a system which at $t=0$ occupies a 2-dimensional phase space

$0 < x, y < L$. Suppose that by some means this thermostatted system is subject to a dissipative external field which, after initial transients, causes the distribution function, $f(x, y)$, to collapse towards a one dimensional attractor, $x^2 + y^2 = r^2$. At some time t , the distribution function is given by the equation,


$$\begin{aligned} f(x, y, t) &\sim \frac{1}{2\pi r \Delta(t)} ; & r^2 < x^2 + y^2 < (r + \Delta(t))^2 \\ &= 0 & ; & \text{otherwise} \end{aligned} \quad (10.4.5)$$

Further, we suppose that the width of the annulus which forms the distribution function satisfies an equation of motion,

$$\frac{d\Delta(t)}{dt} = -\alpha \Delta(t) \quad (10.4.6)$$

for some positive constant value of α . It is easy to see that in the steady state, $df/dt = \alpha f$, which is the analog of (10.1.4). The phase space distribution function diverges at a constant rate, α . In spite of this, if we compute the phase average of a nonsingular phase variable $B(x, y)$, time averages will **converge** exponentially fast towards their steady state values, $\langle B(t) \rangle - \langle B(\infty) \rangle \sim e^{-\alpha t}$. This example points out that although the distribution function, as computed from the ostensible phase space, may be diverging at a constant rate, steady state phase averages may still be well defined and convergent. The distribution function computed from within the accessible phase space has no singularities, $f_{\text{acc}}(x, y, t) \equiv f(x, y, t) / (2\pi r \Delta(t)) = 1$, $\forall t$, provided, $r^2 < x^2 + y^2 < (r + \Delta(t))^2$. In our example it is always uniform and constant in time. Phase averages are fundamentally functions of phase space distances not of volumes. Indeed the notion of a phase space volume is somewhat arbitrary.

10.5 Green's Expansion for the Entropy

Since the dimension of the accessible phase space decreases to less than the ostensible $2dN$ dimensions, the volume of the accessible phase space, as measured from the ostensible space is zero. The entropy of a system is proportional to the logarithm of the accessible phase volume. Since that volume as determined from the ostensible phase space, is zero, the entropy will diverge to negative infinity. These simple observations explain the divergence of entropy as computed in the ostensible space. Presumably the thermodynamic entropy should be arrived at by integrating over the accessible phase space only. This would remove the apparent divergence. However the determination of the topology of the phase space which is accessible to nonequilibrium steady states is exceedingly complex. Even the dimension of the accessible space is only known approximately. Such a program for the calculation of the nonequilibrium entropy would therefore appear quite hopeless. 

The fine grained entropy as computed from the ostensible phase space dimension has a number of further difficulties. From a quantum mechanical point of view, if a system such as the one depicted in Figure 10.9 is meant to represent argon, it is in violation of the Heisenberg uncertainty principle. The uncertainty principle puts an absolute limit on the degree to which a distribution function can be fractal. There is a lower limit imposed by Planck's constant, to the scale of features in that can be found in phase space. The extreme fineness of the filaments depicted in Figure 10.9 implies extreme sensitivity to external perturbations. The finer the length scale of the phase space structures, the more sensitive those structures will be to external perturbations. If the distribution function is fractal, there is no limit to the smallness of the phase space structures and therefore no limit to the sensitivity of the full distribution function to uncontrolled external perturbations. In an experiment, averaging over an ensemble of possible external fluctuations would of course *wash out* the fine structure below a critical length scale. The precise cut-off value would be determined by the amplitude and spectrum of the external fluctuations. This *washing out* of fine structure provides an ansatz for the computation of the entropy of nonequilibrium steady states.

Evans(1989) described a systematic method for computing the coarse grained entropy of nonequilibrium steady states. The coarse graining is introduced by decomposing the Gibbs (1902) entropy, into terms arising from the partial distribution functions involving correlations of successive numbers of particles. If the expansion is carried out to order N , the total number of particles in the system, the results will of course be identical to the fine-grained Gibbs entropy. The expansion has been tested at equilibrium and it has been found that for densities less than $\sim 75\%$ of the freezing density, the singlet and pair contributions to the entropy appear to be accurate to more than $\sim 90\%$. At equilibrium, the expansion therefore appears to converge rapidly. Away from equilibrium the expansion will consist of a series of finite terms until the dimension of the partial distribution function exceeds the dimension of the accessible phase space. Once this occurs all succeeding terms will be infinite. The method yields finite terms below this dimension because all

the lower dimensional integrals are carried out in the accessible phase space.

H.S. Green used Kirkwood's factorization (1942) of the N-particle distribution function to write an expansion for the entropy. If we define z-functions in an infinite hierarchy, as

$$\begin{aligned}\ln f_1^{(i)} &\equiv z_1^{(i)} \\ \ln f_2^{(ij)} &\equiv z_2^{(ij)} + z_1^{(i)} + z_1^{(j)} \\ \ln f_3^{(ijk)} &\equiv z_3^{(ijk)} + z_2^{(jk)} + z_2^{(ki)} + z_2^{(ij)} + z_1^{(i)} + z_1^{(j)} + z_1^{(k)}\end{aligned}\quad (10.5.1)$$

.....

where the various f-functions are the partial 1,2,3, .. -body distribution functions, then Green showed that Gibbs' fine grained entropy (equation 10.1.1) can be written as an infinite series,

$$S = -k_B \left\{ \frac{1}{1!} \int d\Gamma_1 f_1 z_1 + \frac{1}{2!} \iint d\Gamma_1 d\Gamma_2 f_2 z_2 + \dots \right\} \quad (10.5.2)$$


Using equation (10.5.1) one can easily show that the entropy per particle is given by the following series.

$$\begin{aligned}\frac{S}{N} &= -\frac{k_B}{\rho} \int d\mathbf{p}_1 f_1(\mathbf{p}_1) \ln f_1(\mathbf{p}_1) \\ &\quad - \frac{k_B}{2N} \iint d\Gamma_1 d\Gamma_2 f_2(\Gamma_1, \Gamma_2) \ln \left[\frac{f_2^{(12)}}{f_1^{(1)} f_1^{(2)}} \right] + \dots\end{aligned}\quad (10.5.3)$$

In deriving this equation we have assumed that the fluid is homogeneous. This enables a spatial integration to be performed in the first term. This equation is valid away from equilibrium. Using the fact that at equilibrium the two body distribution function factors into a product of kinetic and configurational parts equation (10.5.3) for two dimensional fluids, reduces to,

$$\frac{S}{N} = 1 - k_B \ln \left(\frac{\rho}{2\pi m k_B T} \right) - \frac{k_B \rho}{2} \int d\mathbf{r}_{12} g(r_{12}) \ln g(r_{12}) + \dots \quad (10.5.4)$$

where $g(r_{12})$ is the equilibrium radial distribution function. Equation (10.5.4) has been tested using experimental radial distribution function data by Mountain and Raveché (1971) and by Wallace (1987). They found that the Green expansion for the entropy, terminated at the pair level, gives a surprisingly accurate estimate of the entropy from the dilute gas to the freezing density. As far as we know prior to Evans' work in 1989, the Green expansion had never been used in computer simulations. This was because, in the canonical ensemble, Green's entropy expansion is non-local.

In Evans' calculations the entropy was calculated by integrating the relevant distribution functions over the **entire** simulation volume. A recent reformulation of (10.5.4) by Baranyai and Evans, (1989), succeeds in developing a local expression for the entropy of a canonical ensemble of systems. Furthermore the Baranyai-Evans expression for the entropy is ensemble independent. 

Evans (1989), used a simulation of 32 soft discs ($\phi(r) = \epsilon(\sigma/r)^{12}$ truncated at $r/\sigma=1.5$) to test equation (10.5.4) truncated at the pair level. All units were expressed in dimensionless form by expressing all quantities in terms of the potential parameters σ, ϵ and the particle mass m . Table 10.3, below shows some of the equilibrium data gathered for the soft disc fluid. All units are expressed in reduced form. Each state point was generated from a ten million timestep simulation run using a reduced timestep of 0.002. The energy per particle is denoted e , and the total 1 and 2-body entropy per particle is denoted by s . The entropy was calculated by forming histograms for both $g(\mathbf{r})$ and $f(\mathbf{p})$. These numerical approximations to the distribution functions were then integrated numerically. The radial distribution function was calculated over the minimum image cell to include exactly the long ranged, nonlocal, contributions arising from the fact that at long range, $g(r) = (N-1)/N$. The equipartition, or kinetic, temperature corrected for $O(1/N)$ factors, is denoted by T_k . The thermodynamic temperature T_{th} was calculated from equation (10.5.4) using the thermodynamic relation, $T_{th} = \partial e / \partial s)_V$. For each density the three state points were used to form a simple finite difference approximation for the derivative.

The analytical expression for the kinetic contribution to the entropy was not used, but rather this contribution was calculated from simulation data by histogramming the observed particle velocities and numerically integrating the single particle contribution. The numerical estimate for the kinetic contribution to the entropy was then compared to the theoretical expression (basically the Boltzmann H-function) and agreement was observed within the estimated statistical uncertainties.

By using the entropies calculated at $\rho = 0.6, 0.7$ to form a finite difference approximation to the derivative $\partial s / \partial \rho^{-1}$ one can compare the pressure calculated from the

relation $p = T \partial S / \partial V)_E$, with the virial expression calculated directly from the simulation. The virial pressure at $e=2.134, \rho=0.65$, is 3.85 whereas the pressure calculated exclusively by numerical

Table 10.3. Equilibrium moderate density data

ρ	e	s	T_k	T_{th}
0.6	1.921	3.200		
0.6	2.134	3.341	1.552	1.614
0.6	2.347	3.464		
0.625	1.921	3.034		
0.625	2.134	3.176	1.499	1.500
0.625	2.347	3.318		
0.65	1.921	2.889		
0.65	2.134	3.044	1.445	1.454
0.65	2.347	3.182		
0.675	1.921	2.754		
0.675	2.134	2.919	1.306	1.374
0.675	2.347	3.064		
0.7	1.921	2.889		
0.7	2.134	3.044	1.326	1.291
0.7	2.347	3.182		

The uncertainties in the entropies are ± 0.005 .

differentiation of the entropy is 3.72 ± 0.15 . The largest source of error in these calculations is likely to be in the finite difference approximation for the various partial derivatives.

Away from equilibrium the main difficulty in using even the first two terms in equation (10.5.3) is the dimensionality of the required histograms. The nonequilibrium pair distribution function does **not** factorize into a product of kinetic and configurational parts. One has to deal with the full function of 6 variables for translationally invariant two dimensional fluid. In his work, Evans reduced the density to $\rho \sim 0.1$ where the configurational contributions to the entropy should be unimportant. He evaluated the entropy of the same system of 32 soft discs, but now the system was subject to isoenergetic planar Couette flow, using the SLLOD equations of motion. In this simulation a constant thermodynamic internal energy $H_0 \equiv \Sigma p^2/2m + \Phi$ was maintained. The thermostating multiplier α , takes the form (see equation 5.2.3),

$$\alpha = - \frac{P_{xy} \gamma V}{\sum \frac{p_i^2}{m}} \quad (10.5.5)$$

where P_{xy} is the xy-element of the pressure tensor.

To check the validity of our assumption that at these low densities, the configurational parts of the entropy may be ignored, he performed some checks on the equilibrium thermodynamic properties of this system. Table 10.4 shows the thermodynamic temperature computed using a

finite difference approximation to the derivative, $\partial e/\partial s$, ($e=\langle H_0 \rangle/N$, $s=S/N$). It also shows the kinetic temperature computed using the equipartition expression. At equilibrium, the data at a reduced density of 0.1 predicts a thermodynamic temperature which is in statistical agreement with the kinetic temperature, 2.12 ± 0.04 as against 2.17, respectively. The equilibrium data at $e=2.134$, $\rho=0.1$, gives a thermodynamic pressure of 0.22, in reasonably good agreement with the virial pressure (including both kinetic and configurational components) of 0.24. The disagreement between the thermodynamic and the kinetic expressions for both the temperature and the pressure arise from two causes; the absence of the configurational contributions, and the finite difference approximations for the partial derivatives.

Figure 10.14 shows the analogue of Figure 10.9 for a 32 particle system under shear. The nonequilibrium pair distribution function is free of the singularities apparent in the 2-particle system. The reason why it is smooth is that for 1 and 2-particle distributions in systems of many particles, one averages over all possible positions and momenta for the other $N-2$ particles. This averaging *washes out* the fine structure. These distributions even at very high strain rates, are **not** fractal. If the Green expansion converges rapidly we will clearly arrive at a finite value for the entropy.

Table 10.4 gives the computed kinetic contribution to the entropy as a function of energy, density and strain rate. At low densities the increased mean free paths of particles relative to the corresponding situation in dense fluids means that considerably longer simulation runs are required to achieve an accuracy comparable to that for dense fluids. The data given in table 10.4 is taken from 15 million timestep simulation runs. Away from equilibrium the strain rate tends to increase the *mixing* of trajectories in phase space so that the errors actually decrease as the strain rate is increased.

For a given energy and density, the entropy is observed to be a monotonically **decreasing** function of the strain rate. As expected from thermodynamics, the equilibrium state has the maximum entropy. Although there is no generally agreed upon framework for thermodynamics far from equilibrium, it is clear that the entropy can be written as a function, $S = S(N, V, E, \gamma)$. **Defining** T_{th} as $\partial E/\partial S)_{V, \gamma}$, p_{th} as $T \partial S/\partial V)_{E, \gamma}$ and ζ_{th} as $-T \partial S/\partial \gamma)_{E, V}$, we can write,

$$dE = T_{th} dS - p_{th} dV + \zeta_{th} d\gamma \quad \text{[Equation Icon]} \quad (10.5.6)$$

Some years ago Evans and Hanley (1980) proposed equation (10.5.6) as a generalized Gibbs relation, however, at that time there was no way of directly computing the entropy or any of the free energies. This forced Evans and Hanley to postulate that the thermodynamic temperature was equal to the equipartition or kinetic temperature, $T_k \equiv 2K/(dNk_B)$, for systems in d dimensions. Evans and Hanley observed that away from equilibrium, although the pressure tensor is anisotropic, the thermodynamic pressure must be independent of the manner in which a virtual volume change is performed. The thermodynamic pressure must therefore be a scalar. They

assumed that the thermodynamic pressure would be equal to the *simplest scalar invariant of the pressure tensor* that was also consistent with equilibrium thermodynamics. In two dimensional systems they assumed that $p=(P_{xx}+P_{yy})/2$.

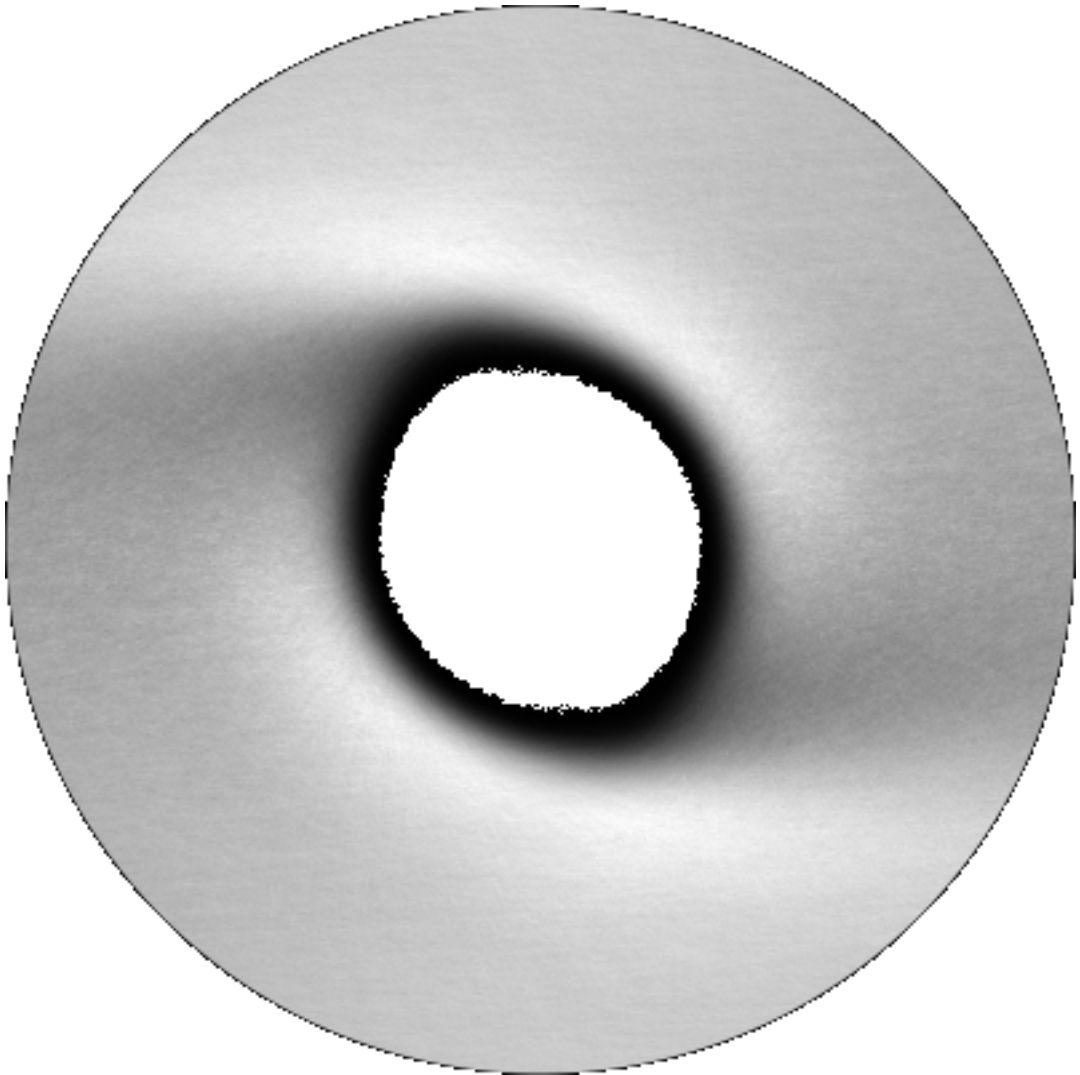


Figure 10.14 Shows the pair distribution function for the 32-particle soft disc fluid at a relatively high reduced strain rate of 2.0. The reduced density and total energy per particle is 0.1, 1.921, respectively. The run length is 24 million timesteps. The distribution is, as far as can be told from the simulation data, completely smooth. In spite of the high anisotropy of this distribution, the configurational contribution to the system entropy is only about 0.4%.

Since we can now calculate the coarse grained Gibbs entropy directly, we can check the correctness of these postulates. We assume, that the internal energy is given by the sum of the peculiar kinetic energy and the potential energy, that we know the system volume and strain rate and that the thermodynamic entropy is equal to the coarse grained Gibbs entropy which at low densities can be approximated by the first term of equation (10.5.3). Table 10.4 below shows a comparison of kinetic and thermodynamic temperatures for the 32-particle soft-disc system.

Table 10.4. Low density data

ρ	γ	e	s	T_k	T_{th}
0.075	0.0	2.134	6.213		
0.1	0.0	1.921	5.812		
0.1	0.0	2.134	5.917(27)	2.175	2.12(6)
0.1	0.0	2.346	6.013		
0.125	0.0	2.134	5.686		
0.075	0.5	1.921	5.744		
0.075	0.5	2.134	5.852	2.190	2.088
0.075	0.5	2.347	5.948		
0.1	0.5	1.921	5.539		
0.1	0.5	2.134	5.653	2.171	2.048
0.1	0.5	2.346	5.747		
0.125	0.5	1.921	5.369		
0.125	0.5	2.134	5.478	2.153	2.088
0.125	0.5	2.347	5.573		
0.075	1.0	1.921	5.380		
0.075	1.0	2.134	5.499	2.188	1.902
0.075	1.0	2.347	5.604		
0.1	1.0	1.921	5.275		
0.1	1.0	2.134	5.392	2.169	1.963
0.1	1.0	2.346	5.492		
0.125	1.0	1.921	5.157		
0.125	1.0	2.134	5.267	2.149	2.019
0.125	1.0	2.347	5.368		

Away from equilibrium the uncertainties in the entropy are ± 0.005 .

As has been known for some time (Evans, 1983), $\partial T_k / \partial \gamma)_{V,E}$ is negative leading to a decrease in the kinetic temperature with increasing strain rate. For this low density system the effect is far smaller than has been seen for moderately dense systems. At a density of 0.1 the kinetic temperature drops by 0.3% as the shear rate is increased to unity. The precision of the kinetic temperature for these runs is about 0.01%. The thermodynamic temperature also decreases as the strain rate is increased but in a far more dramatic fashion. It decreases by 10% over the same range of strain rates. The results clearly show that away from equilibrium the thermodynamic temperature is smaller than the kinetic or equipartition temperature. As the strain rate increases the discrepancy grows larger.

Using the simulation data at $e=2.134$, one can estimate the thermodynamic pressure as a function of strain rate. Table 10.5 shows the finite difference approximation for the thermodynamic pressure, p_{th} , the hydrostatic pressure, $p_{tr} = (P_{xx} + P_{yy})/2$ and the largest and

smallest eigenvalues of the pressure tensor p_1, p_2 respectively. As expected the hydrostatic pressure increases with shear rate. This effect, known as shear dilatancy, is very slight at these low densities. The thermodynamic pressure shows a much larger effect but it **decreases** as the strain rate is increased. In an effort to give a mechanical interpretation to the thermodynamic pressure we calculated the two eigenvalues of the pressure tensor. Away from equilibrium, the diagonal elements of the pressure tensor differ from one another and from their equilibrium values, these are termed normal stress effects. The eigenvalues are influenced by all the elements of the pressure tensor including the shear stress. One of the eigenvalues increases with strain rate while the other decreases and within statistical uncertainties the latter is equal to the thermodynamic pressure.

Table 10.5. Nonequilibrium pressure.

$e=2.134, \rho=0.1$

γ	p_{th}	p_{tr}	p_1	p_2
0.0	0.215(7)	0.244	0.244	0.244
0.5	0.145	0.245	0.361	0.130
1.0	0.085	0.247	0.397	0.096

Evans(1989) conjectured that the thermodynamic pressure is equal to the minimum eigenvalue of the pressure tensor, that is $p_{th} = p_2$. This relation is exact at equilibrium and is in accord with our numerical results. It is also clear that if the entropy is related to the minimum reversible work required to accomplish a virtual volume change in a nonequilibrium steady state system, then $p_2 dV$ is the minimum pV work that is possible. If one imagines carrying out a virtual volume change by moving walls inclined at arbitrary angles with respect to the shear plane then the minimum virtual pV work (minimized over all possible inclinations of the walls) will be $p_2 dV$.

Figure 10.15 shows the kinetic contribution to the entropy as a function of strain rate for the 32-particle system at an energy $e=2.134$ and a density $\rho=0.1$. The entropy seems to be a linear function of strain rate for the range of strain rates covered by the simulations. Combining these results with those from Table 10.4 allows us to compute ζ_{th} as a function of strain rate. For $\gamma=0.0, 0.5, 1.0$ we find that $\zeta_{th}/N = 1.22, 1.08, \text{ and } 0.91$ respectively. Most of the decrease in ζ is due to the decrease in the thermodynamic temperature with increasing strain rate. We have assumed that asymptotically s is linear in strain rate as the strain rate tends to zero. It is always possible that at strain rates which are too small for us to simulate, that this linear dependence gives way to a quadratic variation.

Although these calculations are restricted to the low density gas regime, the results suggest that a sensible definition for the nonequilibrium entropy can be given. A definition, based on equation (10.5.3), avoids the divergences inherent in the fine grained entropy due to the

contraction of the nonequilibrium phase space. At low densities this entropy reduces to the Boltzmann entropy implicit in the Boltzmann H-function. Our entropy is, for states of a specified energy and density, a maximum at equilibrium.

Defining a temperature on the basis of this entropy, indicates that far from equilibrium there is no reason to expect that the equipartition, or kinetic temperature is equal to the thermodynamic temperature. Similarly there seems to be no reason to expect that the average of the diagonal elements of the pressure tensor will be equal to the thermodynamic pressure far from equilibrium. The concept of minimum reversible virtual work, together with our numerical results suggests that the thermodynamic pressure is instead equal to the minimum eigenvalue of the pressure tensor.

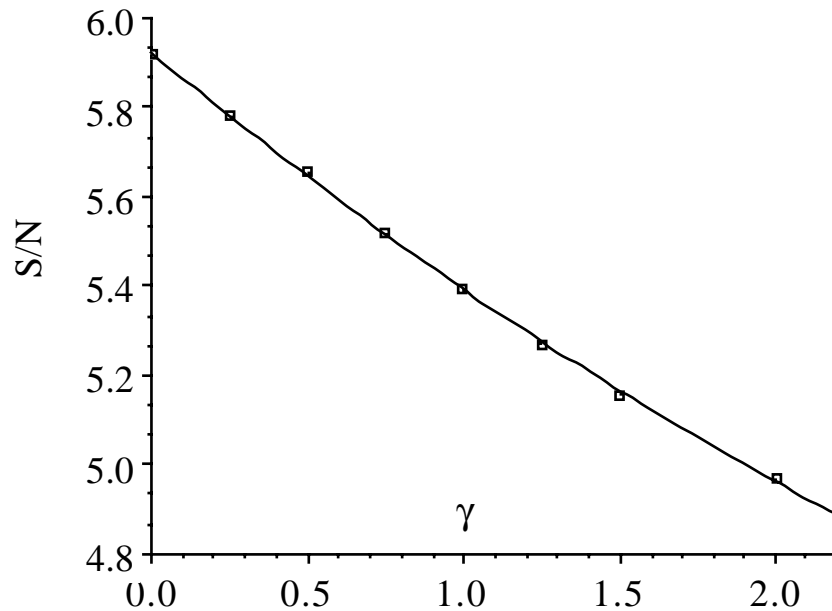


Figure 10.15 Shows the kinetic contribution to the system entropy as a function of strain rate. The system density is 0.1 and the energy per particle is 2.134. Within the accuracy of the data the entropy is essentially a linear function of strain rate. The derivative of the entropy with respect to strain rate gives ζ/T . ζ is positive but decreases with strain rate, mostly due to the decrease in the thermodynamic temperature with increasing strain rate.

One can form an exact fluctuation expression for our nonequilibrium entropy. In the low density regime one can use the exact time correlation function formalism (§7.3) to show that the single particle velocity distribution is related to transient correlations of the equilibrium stress, $-P_{xy}(0)$ and the transient probability that at a time s , a particle had a momentum \mathbf{p} .

$$f_{SS}(\mathbf{p}) = f_{eq}(\mathbf{p}) \left\{ 1 - \beta \gamma V \int_0^{\infty} ds P_{xy}(0) f(s; \mathbf{p}) \right\} \quad (10.5.7)$$

In this equation f_{SS} is the steady state single particle distribution function. It is equal to the limit as $s \rightarrow \infty$, of $f(s; \mathbf{p})$. f_{eq} is the initial equilibrium Maxwell-Boltzmann distribution with Boltzmann factor $\beta = 1/k_B T$, (note: $f(s=0; \mathbf{p}) = f_{eq}$). Equation (10.5.7) may be substituted into the first term of (10.5.3), to give an exact expression for the low density entropy. It can then be used to compute various inter-relationships between entropy derivatives. It remains to be seen whether the entropy so defined, is a local maximum in nonequilibrium steady states. If this can be satisfactorily demonstrated then we will have for the first time a fundamental basis for a generalized thermodynamics of steady states far from equilibrium.